New Calculation of Fission Barriers for Heavy and Superheavy Nuclei*

M. Bolsterli, E. O. Fiset,† J. R. Nix, and J. L. Norton
Los Alamos Scientific Laboratory, University of California, Los Alamos, New Mexico 87544

(Received 8 November 1971)

On the basis of the macroscopic-microscopic method we have performed a new calculation of the nuclear potential energy of deformation for heavy and superheavy nuclei. Our primary emphasis has been to develop techniques that permit more accurate extrapolations both to the large deformations encountered in fission and heavy-ion reactions and to new regions of nuclei. With this purpose in mind, we specify the nuclear shape with five degrees of freedom, in terms of smoothly joined portions of three quadratic surfaces of revolution (e.g., two spheroids connected by a hyperboloidal neck). The single-particle potential is obtained by folding a Yukawa function with a uniform sharp-surface generating potential of appropriate shape. The parameters describing the potential are obtained from statistical (Thomas-Fermi) calculations that reproduce correctly the average trends throughout the Periodic Table of a variety of nuclear properties. To solve the Schrödinger equation for the single-particle energies and wave functions, we have used mainly an expansion of the wave function in a set of deformed harmonic-oscillator basis functions, but have also investigated a finite-difference method. Shell and pairing corrections are calculated from the single-particle energies by means of the methods developed by Strutinsky and added to the surface and Coulomb energies of the liquid-drop model to obtain the total potential energy of deformation.

This approach is found to reproduce reasonably well the over-all trends of experimental fission-barrier heights of nuclei ranging from rare earths to actinides. The calculated fission barriers of actinide nuclei contain two peaks separated by a secondary minimum. The over-all variation in the relative heights of the two peaks agrees with experimental results, but the calculated first peak is somewhat low for thorium isotopes and somewhat high for curium isotopes. For the actinides the first saddle point is found to be symmetric in shape and the second saddle point asymmetric. The highest saddle point is asymmetric for ^{226}Ra and ^{210}Po and symmetric for ^{188}Os. The fission barriers of superheavy nuclei near ^{298}114 are even higher than previously supposed. With respect to spontaneous fission, the island of superheavy nuclei is a mountain ridge extending from 114 protons to about 124 protons. The descent from the mountain down to the sea of instability is rather gentle for decreasing neutron numbers below 184, but is more rapid on the other three sides.

I. INTRODUCTION

Over the years, considerable effort has been devoted to calculating the potential energy of a nucleus as a function of its neutron and proton numbers and its shape. The over-all trends of the nuclear potential energy are described quantitatively by the liquid-drop model, but there are regular deviations from the liquid-drop energy. The most striking deviation is associated with shell effects: Closed-shell nuclei are more tightly bound than an "average" nucleus, while midshell nuclei are less tightly bound. The second most important deviation is associated with nuclear pairing, which also leads to increased binding in some nuclei relative to others. These shell and pairing corrections to the liquid-drop energy are both examples of single-particle effects, and arise because of fluctuations in the actual distribution of single-particle levels in the nucleus relative to a smooth distribution of levels. Recently, quantitative theories of these corrections have been proposed,[1,2] and numerous calculations have already been carried out.[3-74]

Single-particle effects are responsible for many familiar and important phenomena. These include the occurrence of deformed rather than spherical ground-state shapes for midshell nuclei, and the occurrence of secondary minima in the fission barriers of some actinide nuclei. These secondary minima may be responsible for the recently discovered fission isomers and intermediate structure in fission cross sections. Also, the division of heavy nuclei at low excitation energies into fragments of *unequal* mass is believed to be caused by single-particle effects. Finally, the possibility that there may exist an island of relatively stable superheavy nuclei near 114 protons and 184 neutrons is due to the extra stability arising from shell closures in that region.

Of course, the most fundamental approach for calculating the nuclear potential energy would be to start with a nucleon-nucleon interaction and solve the resulting many-body equations in some

approximation. However, such fundamental approaches have not yet achieved the accuracy of a two-part approach based on adding shell and pairing corrections to the liquid-drop energy. (We omit throughout the paper bibliographic citations to work based on more fundamental self-consistent approaches.) In the macroscopic-microscopic method,[1-74] which we use here, the total nuclear potential energy E is given by

$$E(N,Z,\text{shape}) = E_{\text{ld}}(N,Z,\text{shape}) + \Delta E_{\text{sc}}(N,Z,\text{shape}) + \Delta E_{\text{pc}}(N,Z,\text{shape}), \quad (1)$$

that is, by the sum of a liquid-drop energy E_{ld}, a shell correction ΔE_{sc}, and a pairing correction ΔE_{pc}. The liquid-drop term gives the smooth trends of the potential energy, while the shell and pairing corrections, which are calculated from single-particle energies, give the fluctuations about the smooth trends.

In addition to the *potential* energy given by Eq. (1), a complete theory of phenomena associated with shape changes would of course also require that the kinetic energy be known. However, we limit our discussion here to the potential energy.

The basic problem we consider is the computation of the nuclear potential energy as a function of shapes appropriate to nuclei undergoing fission, such as the shapes illustrated in Fig. 1. Figure 2 shows the general dependence of the potential energy on such shapes for a heavy nucleus like ^{240}Pu. The smooth trends of the curve are described by the liquid-drop term E_{ld}, and the small wiggles by the shell and pairing corrections ΔE_{sc} and ΔE_{pc}.

In addition to fission, the techniques developed here are also applicable to calculating the potential energy for shapes involved in the collision of two heavy ions, such as in attempts to produce superheavy nuclei. However, we do not present here any results concerning heavy-ion reactions.

In calculating the nuclear potential energy, we take the liquid-drop part from previous work.[4,75] Since the shell and pairing corrections depend upon the single-particle levels near the Fermi surface, our main emphasis is on the accurate calculation of these levels for large deformations and in new regions of nuclei.

The procedure for determining the single-particle levels in general consists of three steps: (1) specifying the over-all geometrical shape of the nucleus, (2) generating single-neutron and single-proton potentials related to this shape, and (3) solving the Schrödinger equation with these potentials for the single-particle levels. Various aspects of these steps have recently been considered by several groups.[2,7-70,76-95]

In our work, we have tried at each step to develop from the outset techniques suited to large deformations and to new regions of nuclei. With this goal in mind, we have proceeded as follows:
(1) To describe adequately the deformed shapes of interest in fission and in heavy-ion reactions, we

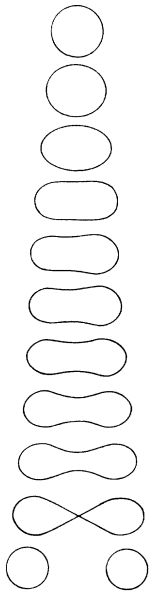

FIG. 1. Nuclear shapes involved in fission.

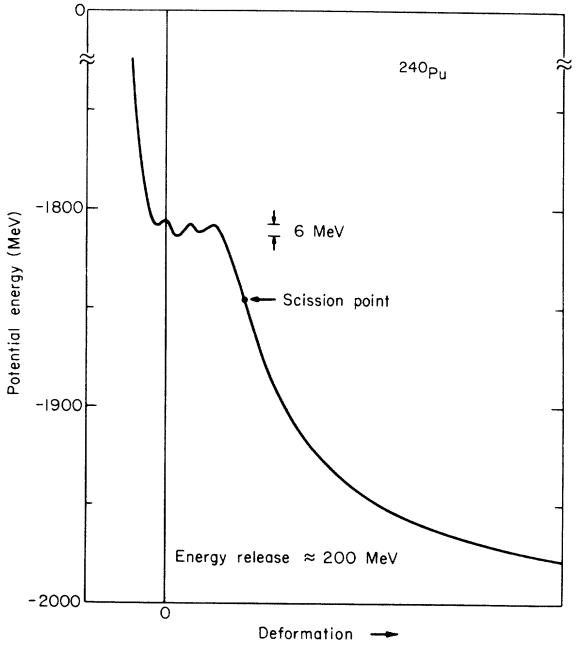

FIG. 2. Dependence of potential energy on deformation in the fission degree of freedom.

specify the nuclear shape with five degrees of freedom, in terms of smoothly joined portions of three quadratic surfaces of revolution (e.g., two spheroids connected by a hyperboloidal neck).[75]

(2) To obtain a single-particle potential that is everywhere related physically to the given shape, we fold a Yukawa function with a uniform sharp-surface generating potential of appropriate shape.[67-70,91-95] The parameters of the potential are obtained from statistical (Thomas-Fermi) calculations that reproduce correctly average trends throughout the Periodic Table of such nuclear properties as total binding energy, saturation density, and surface diffuseness.[96]

(3) To solve the Schrödinger equation for the single-particle energies we have used both an expansion of the wave function in a set of deformed harmonic-oscillator wave functions[17,22,80,90,91] and also a finite-difference method.[81,92,93] We had initially thought that the finite-difference method would be preferable for very large deformations, but this turned out not to be the case. We have therefore used the expansion method for most of our calculations.

Once the single-particle levels have been computed for both neutrons and protons at a given deformation, the shell and pairing corrections are calculated from them by means of the methods suggested by Strutinsky.[7-70] The total potential energy is then given by the sum of the liquid-drop energy and the shell and pairing corrections.

As an outline of what is to follow, we discuss the description of nuclear shapes in Sec. II, the generation of the single-particle potential in Sec. III, and the calculation of the single-particle energies and wave functions in Sec. IV. The various terms in the potential energy of deformation are described in Sec. V. Section VI contains the fission barriers for heavy and superheavy nuclei that have been calculated thus far with this approach. Section VII summarizes and concludes this initial portion of our study.

II. NUCLEAR SHAPES

A general theory of the shape dependence of the nuclear Hamiltonian should be capable of discussing within the same framework the related areas of fission, nuclear ground-state masses and deformations, and heavy-ion reactions. In fission it is necessary to be able to describe in a continuous way the sequence of shapes of a fissioning nucleus from its ground state, through its saddle and scission configurations, to the separated fragments at infinity, including asymmetric shapes (see again Fig. 1). In a study of ground-state shapes one must be able to describe a sphere, oblate and prolate spheroids, octupole deformations, and positive and negative hexadecapole deformations. In the fusion of two heavy ions it is necessary in addition to be able to describe configurations such as two tangent spherical nuclei. In all cases, the coordinates used to describe the nuclear shapes should be related to quantities of physical interest. Since many phenomena of interest do not depend sensitively upon deviations from axial symmetry, we specialize immediately to shapes that are axially symmetric.

With the above in mind, we choose to consider a total of five coordinates and specify the nuclear shape in terms of smoothly joined portions of three quadratic surfaces of revolution. (In different terminology, the nuclear shape is defined in terms of a second-degree spline function of revolution). Figure 3 illustrates such a shape, formed from two spheroids connected by a hyperboloidal neck.[75] In terms of a cylindrical coordinate system, the equation for the drop's surface is written explicitly as

$$\rho^2 = \begin{cases} a_1^2 - (a_1^2/c_1^2)(z-l_1)^2, & l_1 - c_1 \leq z \leq z_1 \\ a_2^2 - (a_2^2/c_2^2)(z-l_2)^2, & z_2 \leq z \leq l_2 + c_2 \\ a_3^2 - (a_3^2/c_3^2)(z-l_3)^2, & z_1 \leq z \leq z_2 . \end{cases}$$

As shown in Fig. 3, the quantity l_i specifies the position of the center of the ith quadratic surface, c_i its semisymmetry axis, and a_i its transverse semiaxis ($i = 1, 2, 3$).

At this stage there are nine coordinates in the specification of the nuclear shape. However, one coordinate is eliminated by our assumption that the volume remain constant, and two more by the requirement that the middle surface join smoothly with each of the two end surfaces (at the points denoted by z_1 and z_2). This introduces three relationships between the original nine degrees of freedom, and reduces the number to six. Elimination of the center-of-mass coordinate finally reduces

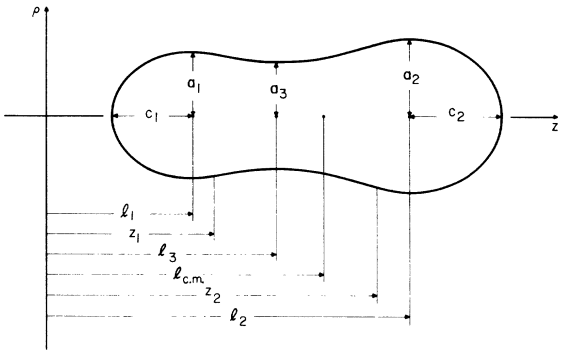

FIG. 3. Shape described by two spheroids connected by a hyperboloidal neck.

the number of shape coordinates to five. (In practice it is often better to retain the center-of-mass coordinate at this point and eliminate it implicitly later.)

Of these five coordinates, three describe symmetric deformations, and the remaining two asymmetric deformations. The most important symmetric coordinate is the over-all fission or separation coordinate, which describes the distortion of the fissioning nucleus from its ground state, through its saddle and scission configurations, to the separated fragments at infinity. (The relevant separation coordinate is somewhat different for the the fusion of two heavy ions than for fission.) The most important asymmetric coordinate is the mass-asymmetry coordinate, which describes the amount of mass in one side of the nucleus relative to the other. The remaining coordinates describe such quantities as the neck radius and the eccentricities of the ends of the nucleus. (The actual coordinates being used are defined in Ref. 75.)

The precise determination of the fission coordinate would require performing a dynamical calculation. However, during the early stages of fission the symmetric-deformation coordinate y introduced by Hill and Wheeler[97] provides a fair approximation to the fission coordinate. This coordinate, which is the same as the coordinate t used by Swiatecki,[98] is defined in terms of the saddle-point shapes for an idealized uniformly charged liquid drop; specifically, the saddle-point shape corresponding to a given value of the fissility parameter x represents a deformation of

$$y = 1 - x .$$

Thus, as y ranges from 0 to 1, the sequence of shapes ranges from a single sphere through symmetric dumbbell-like shapes to two tangent spheres. For values of y between 0 and 0.4 these deformations are illustrated in Fig. 4 by the shapes on the left-hand side.[67,68,92] To first order, y is related to the coordinates that describe prolate spheroidal and Legendre-polynomial P_2 distortions by

$$y = \tfrac{1}{7}e^2 = \tfrac{2}{7}\epsilon = \tfrac{2}{7}\delta = \tfrac{3}{7}\alpha_2 = \frac{3}{7}\left(\frac{5}{4\pi}\right)^{1/2}\beta \approx 0.270\beta .$$

The advantage of the coordinate y over other one-parameter fission coordinates is that it includes automatically the liquid-drop-model saddle-point shape for all nuclei, which is fairly close to the actual equilibrium configurations of interest. However, it should be stressed that this coordinate represents approximate distortions in the fission direction only for moderate values of $y \lesssim 0.4$, and we will be using it in this region only. (At $y = 0.437$, which is the point where the derivatives of the relative surface and Coulomb energies with respect to y change sign,[75] the liquid-drop potential energy plotted vs y has a spurious equilibrium configuration.[98] For larger values of y this coordinate therefore does not describe motion in the fission direction.) Although most of the results presented here are in terms of the coordinate y, we have also considered other deformations, especially mass-asymmetric deformations.

It should be emphasized from the outset that the present parametrization is deficient in two important respects. First, it is not particularly well

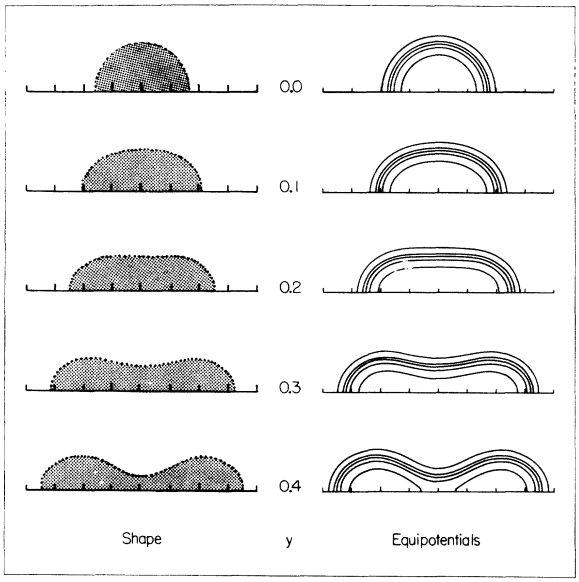

FIG. 4. Shapes described by the symmetric-deformation coordinate y, and resulting equipotentials of the folded Yukawa spin-independent nuclear potential V_1. The equipotential curves shown are for 10, 30, 50, 70, and 90% of the well depth V_0.

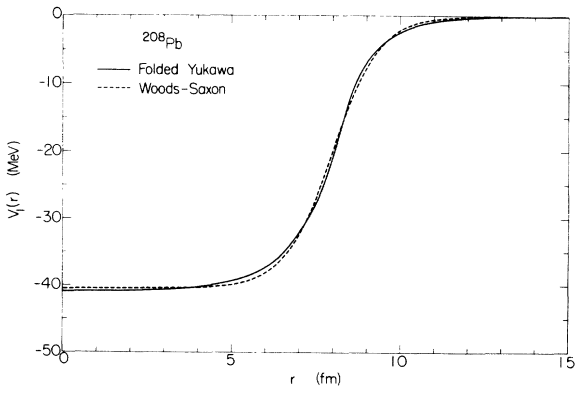

FIG. 5. Comparison of folded Yukawa spin-independent nuclear potential with Woods-Saxon potential for neutrons in a spherical ^{208}Pb nucleus.

suited for describing small deviations from a spherical or a spheroidal shape,[75] which makes it difficult to use in a detailed discussion of nuclear ground-state masses and equilibrium deformations. (For example, in order to describe *positive* hexadecapole or diamond-like deformations, one of the coordinates of Ref. 75 must assume an imaginary value, and the corresponding formulas must be generalized. This has not yet been done, but is planned for the near future.) Second, the parametrization is unable to describe shapes with more than one neck or to describe division into more than two bodies, which makes it impossible to discuss ternary fission.

III. SINGLE-PARTICLE POTENTIAL

A. General Features

Once the nuclear shape has been specified, the next step is to generate single-neutron and single-proton potentials related to that shape. If the procedure is to be useful in a general theory of fission, it must be capable of handling very deformed shapes, and in particular the transition from *one* original nucleus to *two* (or more) final fragments.

For the initial ground-state nucleus we know that the nuclear spin-independent part of the single-particle potential (for either neutrons or protons) is roughly constant in the nuclear interior and rises to zero in a small distance near the nuclear surface. After fission has occurred, the potential has similar features concentrated in each of the separated fragments. This means that during the intermediate stages the potential must remain nearly constant in the interiors of the nascent fragments and approach zero in the neck region. The over-all geometrical shape of the potential is expected to change in roughly the same manner as that of the nucleus.

To guarantee in a simple way that the potential has these properties, we generate it by means of the following two steps: (1) We start with a uniform sharp-surface "generating potential" whose shape corresponds to the given nuclear shape. In other words, the generating potential has the value $-V_0$ inside the specified surface and 0 outside. (2) A potential with a diffuse surface is then obtained by folding a Yukawa function over the sharp generating potential. The Yukawa function is normalized so that its volume integral is unity, and its range is chosen to reproduce the desired surface diffuseness in the final potential. In this way the volume integral of the final potential remains equal to that of the sharp generating potential. This volume integral is assumed to remain constant as the shape is changed.

(In our earlier publications,[67-70,92] we have described this method of generating the potential in terms of folding a Yukawa effective two-nucleon interaction with a uniform sharp-surface "pseudo-density" appropriate to the given shape. This terminology unfortunately causes many people to try to identify the pseudodensity with the true nuclear density, and has therefore been abandoned.)

Figure 5 shows that for a spherical shape the potential generated by this folding procedure is very close to a Woods-Saxon potential.[67,68,92] For a spherical shape these two potentials are about equally satisfactory, but for deformed shapes the folded Yukawa potential generalizes in a more natural way than does the Woods-Saxon potential. With the folding procedure it is easy to generate a potential for all the conceivable shapes of interest in fission, including the transition at the scission point to a potential concentrated in each of the two (or more) fission fragments. In this respect our potential serves the same purpose as a generalized two-center harmonic-oscillator potential,[55-57,59-65,83-88] and in addition is far more realistic. As shown on the right-hand side of Fig. 4, the folded Yukawa potentials for deformed shapes are well behaved in the entire surface region; the potentials remain well behaved even for shapes with small or zero necks. This is to be compared with the difficulties encountered in generalizing a Woods-Saxon potential to shapes with small necks.[30]

Besides the spin-independent part of the potential, there is an additional potential arising from the interaction between the nucleon spin and orbital angular momentum. The simplest form for the spin-orbit interaction that has the right symmetry properties for deformed nuclei is $\vec{\sigma}\cdot\nabla V'\times\vec{p}$, where V' is any local spin-independent scalar function. In spherical nuclei this reduces to the familiar $\vec{l}\cdot\vec{s}$ spin-orbit coupling. For V' we have used the spin-independent potential described above.

Finally, protons feel an additional Coulomb interaction; this is calculated by assuming that the protons are distributed uniformly over the same shape and volume as the generating potential.

B. Detailed Formulation

To be more specific, the complete potential felt by a nucleon is given by

$$V = V_1 + V_{so} + V_C .$$

The spin-independent nuclear part is

$$V_1(\vec{r}) = -\frac{V_0}{4\pi a^3}\int_V \frac{e^{-|\vec{r}-\vec{r}'|/a}}{|\vec{r}-\vec{r}'|/a}\,d^3r' , \qquad (2)$$

where V_0 is the well depth felt by either a neutron or a proton, and a is the range of the Yukawa fold-

ing function. The integration is over the volume of the shape, whose magnitude is kept fixed as the shape is deformed. The volume integral of the potential is given by

$$\int_\infty V_1(\vec{r})d^3r = -V_0\tfrac{4}{3}\pi R_0^3,$$

where R_0 is the radius of the spherical sharp-surface generating potential. This result is obtained by substituting Eq. (2) for $V_1(\vec{r})$ and interchanging the order of integrations.

The spin-orbit term is

$$V_{so}(\vec{r}) = -\lambda(\hbar/2mc)^2\vec{\sigma}\cdot\nabla V_1\times\vec{p}/\hbar,$$

where λ is the spin-orbit interaction strength, and m is the mass of either a neutron or a proton. Finally, the Coulomb potential for protons is

$$V_C(\vec{r}) = \frac{Ze^2}{\frac{4}{3}\pi R_0^3}\int_V \frac{d^3r'}{|\vec{r}-\vec{r}'|}. \tag{3}$$

These volume integrals are easily transformed into surface integrals by use of Gauss's divergence theorem. Equations (2) and (3) become

$$V_1(\vec{r}) = -\frac{V_0}{4\pi}\int_S\left[1-\left(1+\frac{|\vec{r}-\vec{r}'|}{a}\right)e^{-|\vec{r}-\vec{r}'|/a}\right]d\Omega',$$

and

$$V_C(\vec{r}) = \frac{1}{2}\frac{Ze^2}{\frac{4}{3}\pi R_0^3}\int_S|\vec{r}-\vec{r}'|^2 d\Omega',$$

where $d\Omega'$ denotes an element of solid angle; the integration is over the surface of the generating potential. In practice we have evaluated these two-dimensional integrals numerically by use of Gaussian quadrature rules. (The result for the Coulomb potential can be further reduced to a one-dimensional integral whose integrand involves complete elliptic integrals of the first and second kinds,[75,97] but we have found it convenient to retain analogous expressions for V_1 and V_C.)

For a spherical shape, the integrations in Eqs. (2) and (3) can be performed explicitly to give[94,95]

$$V_1(r) = -V_0\left[1-\left(1+\frac{R_0}{a}\right)e^{-R_0/a}\frac{\sinh(r/a)}{r/a}\right], \qquad r\le R_0$$

$$= -V_0\left[\frac{R_0}{a}\cosh\frac{R_0}{a}-\sinh\frac{R_0}{a}\right]\frac{e^{-r/a}}{r/a}, \qquad r\ge R_0$$

and

$$V_C(r) = \frac{1}{2}\frac{Ze^2}{R_0}\left[3-\left(\frac{r}{R_0}\right)^2\right], \quad r\le R_0$$

$$= \frac{Ze^2}{r}, \qquad r\ge R_0.$$

The potentials V_1 and V_C generated in this way are continuous in their values and first derivatives at the surface of the generating potential, but are discontinuous in their second and higher derivatives.

C. Parameters

The single-particle potentials generated by our folding procedure contain a total of five parameters: the neutron well depth V_n, the proton well depth V_p, the radius R_0 of the spherical generating potential, the Yukawa range a, and the spin-orbit interaction strength λ. (For both neutrons and protons we use the same radius R_0, the same range a, and the same spin-orbit strength λ.)

We attempted originally to determine these parameters by calculating the single-particle energies for the four doubly-closed-shell nuclei, ^{208}Pb, ^{48}Ca, ^{40}Ca, and ^{16}O, and adjusting the parameters to optimally reproduce the experimental single-particle energies. However, these attempts suggested that parameters obtained by adjusting to single-particle levels cannot be extrapolated in a physical way. This is because experimental single-particle levels are influenced by many effects not explicitly taken into account in a static single-particle potential. In an attempt to compensate for these effects, the available parameters adjust themselves to values that differ from known experimental information. For example, the neglect of momentum dependence in the potential is partially absorbed by the radius parameter taking on a value that is spuriously small for light nuclei and large for heavy nuclei. Extrapolating a radius parameter obtained in this way to the region of superheavy nuclei would then lead to a value that is substantially larger than the expected value.

In addition, we are mainly interested in calculating the nuclear potential energy of deformation, with applications to nuclear ground-state masses and deformations, to fission barriers of heavy and superheavy nuclei, and to heavy-ion reactions, rather than in nuclear spectroscopy. It is therefore more consistent to use single-particle potentials that are related to these quantities rather than to experimental single-particle levels. Such potentials (apart from the spin-orbit interaction) have recently been determined by Myers on the basis of statistical (Thomas-Fermi) calculations that reproduce correctly the average trends throughout the Periodic Table of a variety of nuclear properties, such as total binding energy, saturation density, and surface diffuseness.[96] The use of these potentials should allow the extrapolations to large deformations and to new regions of nuclei to be made with more confidence than with those obtained by adjusting to single-particle levels.

The potentials determined by Myers are related

by means of an effective two-nucleon force to the macroscopic (liquid-drop) portion of the nuclear energy. Therefore, the number of independent parameters should ultimately be reduced by taking advantage of this relationship. However, the parameters describing the single-particle potential have not yet been made completely consistent with those describing the macroscopic part of the energy, and should therefore be regarded as independent parameters at this stage.

We have decided to use the single-particle potentials determined by Myers, but to increase slightly the neutron and proton well depths to better reproduce the over-all positions of the experimental single-particle levels in ^{208}Pb. Effects associated with the presence of a small neutron skin are neglected. The value of the spin-orbit interaction strength is taken from the work of Blomqvist and Wahlborn.[99]

In using the results of Myers, it is convenient to compute first the auxiliary quantities

$$\bar{\delta} = \frac{(N-Z)/A + 0.0112\,Z^2/A^{5/3}}{1 + 3.15/A^{1/3}},$$

$$\bar{\epsilon} = -\frac{0.147}{A^{1/3}} + 0.330\bar{\delta}^2 + \frac{0.002\,48\,Z^2}{A^{4/3}},$$

and

$$R_\rho = 1.16\,A^{1/3}(1+\bar{\epsilon})\ \text{fm};$$

the physical significance of these quantities is explained in Ref. 96. Then, the five single-particle potential parameters are given by

$$V_n = (52.5 - 48.7\bar{\delta})\ \text{MeV},$$

$$V_p = (52.5 + 48.7\bar{\delta})\ \text{MeV},$$

$$R_0 = R_\rho + 0.82\ \text{fm} - 0.56\ \text{fm}^2/R_\rho,$$

$$a = 0.90\ \text{fm},$$

and

$$\lambda = 32.$$

For the benefit of those accustomed to working with Woods-Saxon potentials, we comment that the spherical half-value radius $R_{1/2}$ is related to the radius R_0 of the spherical generating potential by

$$R_{1/2} = R_0[1 - (a/R_0)^2 + \cdots].$$

Also, the diffuseness parameter a_{WS} of a Woods-Saxon potential having the same 10–90% surface thickness is given by

$$a_{WS} = a\frac{\ln 5}{\ln 9} + \cdots.$$

(In determining the value of a from Myers's results we have not used this relation, but have instead minimized the square of the deviations between Myers's Thomas-Fermi and our folded Yukawa potentials for a semi-infinite distribution.)

IV. SINGLE-PARTICLE ENERGIES AND WAVE FUNCTIONS

Once the potential appropriate to a given shape has been generated, the next step is to solve the two-dimensional Schrödinger equation for the single-particle energies. There are two general methods for doing this: expansion in basis functions and finite-difference methods. We have studied and implemented procedures based upon each of these general methods.

We had originally thought that for very large deformations encountered in the later stages of fission and in heavy-ion reactions, expansion in a limited set of basis functions would lead to large truncation errors and that a finite-difference method would be preferable. We therefore implemented an improved version of the implicit finite-difference method outlined by Dickmann.[81,92,93] Although the procedure works satisfactorily, it turns out that for comparable accuracy in the single-particle energies the finite-difference method requires approximately 25 times as much computing time as the expansion method (for a general reflection-asymmetric axially symmetric shape). We have therefore used the latter method for most of our calculations, including all of those reported here.

In our expansion method, the wave function is expanded in a set of axially symmetric harmonic-oscillator wave functions.[17,22,80,90,91] [In the formulas of Ref. 22, the minus sign in Eq. (19), the factor $\frac{1}{2}$ in Eq. (42), and the square root in Eq. (52) should all be deleted. In addition, Eqs. (52) and (53) both need normalization constants, and parentheses should be inserted around the combination $\Lambda' + \Lambda - 1$ in Eq. (55).] In calculating the matrix elements, the single-particle potential $V(\rho, z)$ is first written as a sum of potentials separable in ρ and z.[91,100] The matrix elements are then calculated numerically by use of Gaussian-Laguerre and Gaussian-Hermite quadrature rules. The matrix elements of the spin-orbit interaction are simplified by using relations between orthogonal polynomials and partial integrations to eliminate derivatives of the potential. For speed and flexibility the matrices are diagonalized by the Givens-Householder method.[101]

For a given shape the deformation of the basis functions is chosen so that the ratio of axes of the spheroid equals the ratio of the half length of the shape to its maximum perpendicular radius (or suitably defined generalizations for asymmetric shapes). The over-all curvature of the basis func-

tions[102] is chosen to yield $\hbar\omega_0 = 41\ \mathrm{MeV}/A^{1/3}$. For a given shape we include all basis functions that have an energy less than or equal to $(N_0 + \frac{3}{2})\hbar\omega_0$, where N_0 denotes the equivalent number of quanta used. [This procedure for determining which basis states are included is identical to that of Refs. 17 and 22, but differs from the traditional method of using (deformed) basis functions corresponding to a definite number of spherical shells.[80, 90, 91]] For single-particle potentials as smooth as our folded Yukawa potential, the convergence of the results as a function of N_0 is much faster than we originally thought, even for large deformations. For calculating the single-particle energies shown later in Figs. 7 and 8, we have used $N_0 = 14$, but the remainder of the calculations have been performed with $N_0 = 12$. Some comments are made in Appendix A on the numerical accuracy of the calculated single-particle energies and wave functions.

For a spherical shape the Schrödinger equation reduces to one dimension, and its solution becomes much easier. For this case we have again implemented both an expansion in a one-dimensional spherical harmonic-oscillator basis and also a standard explicit finite-difference method (the so-called "shooting" method).[99, 103-107] As in the case of two dimensions, the expansion method is several times as fast as the finite-difference method for calculating the single-particle energies with comparable accuracy.

V. POTENTIAL ENERGY OF DEFORMATION

As indicated in Eq. (1), the total potential energy is given in the macroscopic-microscopic method by the sum of the liquid-drop energy, the shell correction, and the pairing correction. In this section we discuss the calculation of these three terms.

A. Liquid-Drop Contribution

For calculating the liquid-drop energy we adopt the smooth part of the mass formula presented by Myers and Swiatecki to the 1966 Lysekil conference.[4] The main reason for this choice is that the ratio of the surface-energy constant to the Coulomb-energy constant is more accurately determined than in other currently available mass formulas. However, recent work by Pauli and Ledergerber[28] suggests that for actinide nuclei this ratio possibly should be about 2% smaller than the value given by Myers and Swiatecki. Since this ratio affects strongly the liquid-drop contribution to the fission barrier, such a decrease would systematically lower our calculated barriers for actinide nuclei by up to 1 MeV.

It is convenient to express the potential energy relative to the energy of a *spherical liquid drop*, which is given by the results of Ref. 4. The two shape-dependent terms that must be considered in the liquid-drop model are the surface energy, which tends to hold the nucleus together, and the Coulomb energy, which tends to pull it apart. This portion of the liquid-drop energy can be written as

$$E_{1d}(N, Z, \text{shape}) = \{[B_s(\text{shape}) - 1] + 2x[B_C(\text{shape}) - 1]\} E_s^{(0)},$$

where the relative surface and Coulomb energies B_s and B_C are functions only of the shape of the nucleus. The dependence on neutron and proton numbers is contained in the spherical surface energy $E_s^{(0)}$ and the fissility parameter x.

Since the nuclear surface is specified in terms of portions of quadratic surfaces of revolution, the relative surface energy B_s can be expressed exactly in terms of elementary transcendental functions. However, the relative Coulomb energy B_C can be reduced at most to a double integral (whose integrand involves complete elliptic integrals of the first and second kinds), which is evaluated numerically by use of Gaussian quadrature rules. The formulas used for computing B_s and B_C are given in Ref. 75.

When the constants of Ref. 4 are used, the surface energy of the spherical drop is given by

$$E_s^{(0)} = 17.9439\left[1 - 1.7826\left(\frac{N-Z}{A}\right)^2\right]A^{2/3}\ \mathrm{MeV}.$$

The fissility parameter, which is defined as the ratio of the Coulomb energy of a spherical sharp-surface drop to twice the spherical surface energy,[3, 4] can then be written as

$$x = \frac{Z^2/A}{50.88\left[1 - 1.7826\left(\frac{N-Z}{A}\right)^2\right]}.$$

In the results reported here, higher-order terms in the expression for the macroscopic energy, such as compressibility and curvature effects,[34, 108-113] are neglected. We plan to take account of such effects in future calculations, when a consistent set of nuclear mass-formula constants are available for specifying their magnitudes.

B. Shell Correction

The shell correction arises because of fluctuations in the actual distribution of single-particle levels relative to a smooth distribution of levels. It is calculated from the single-particle energies at a given deformation by means of the method developed in 1966 by Strutinsky.[2] The basic idea behind such a calculation was first discussed in 1963 by Swiatecki.[1]

Because neutrons and protons independently fill their own set of single-particle orbits, both the shell correction and the pairing correction are given as independent sums of a term for neutrons and an analogous term for protons.

Strutinsky's method for calculating the shell correction seems to work well in practice, but there are still some difficulties justifying it from basic principles. Several quasiderivations of the method[12, 30, 114-116] and a number of different descriptions[2, 7-70] have been given previously. Here we would like to follow a somewhat different, but equivalent, exposition that allows a more intuitive, geometric interpretation of the method, as well as establishes its relationship to some other proposals for calculating shell corrections. Our emphasis is on the single-particle energies[1, 3, 4] themselves rather than on the single-particle level density.

We illustrate the method with the aid of Fig. 6. For a spherical ^{208}Pb nucleus the solid points give the dependence of the calculated single-neutron energies ϵ_n upon the single-particle number n. (Since we increase n by 1 for each *particle*, each doubly degenerate state should in principle be plotted twice; for lack of space on the figure the points corresponding to odd particle numbers are omitted.) For a macroscopic system without single-particle effects all the energies would lie on a smooth curve, but the discreteness of the single particles causes some fluctuations about a monotonic increasing function of n. The discrete energies ϵ_n can be regarded as a "staircase" function $\epsilon_{\text{stair}}(n)$ formed by horizontal and vertical lines through the points.

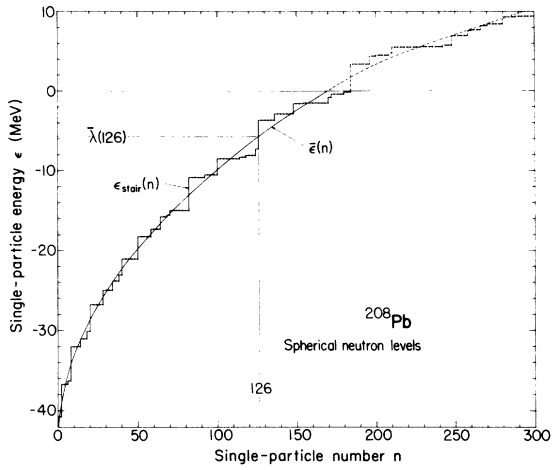

FIG. 6. Dependence of single-neutron energies upon single-particle number for a spherical ^{208}Pb nucleus. The discrete energies are shown by solid points and define a "staircase" function $\epsilon_{\text{stair}}(n)$. The smooth curve $\bar{\epsilon}(n)$ removes the local fluctuations of the solid points, but retains their long-range behavior; it is calculated from Eq. (7) with $p=6$ and $\gamma=1.0\hbar\omega_0=41\ \text{MeV}/A^{1/3}$. The Fermi surface $\bar{\lambda}$ of the smooth distribution of levels is illustrated for 126 neutrons. The corresponding shell correction is given by the difference between the areas under the staircase curve and the smooth curve up to $n=126$. Since the single-particle energies are calculated by use of a finite harmonic-oscillator basis ($N_0=12$), states of positive energy are also discrete; in this region the curves are drawn dashed.

We next remove the local fluctuations of $\epsilon_{\text{stair}}(n)$ while retaining its long-range behavior by passing a smooth curve $\bar{\epsilon}(n)$ through the staircase function. Then the shell correction for a specified particle number N is given simply by the difference between the areas under the staircase curve and the smooth curve up to N, that is,

$$\Delta E_{\text{sc}} = \int_0^N [\epsilon_{\text{stair}}(n) - \bar{\epsilon}(n)]dn = \sum_{n=1}^{N} \epsilon_n - \int_0^N \bar{\epsilon}(n)dn \ . \tag{4}$$

Although we will be calculating shell corrections here only for even particle numbers, this equation also applies to odd values of N.

The description up to this point applies to a general class of shell-correction methods. The various methods in this class[1, 2, 114-119] differ from one another according to the procedure that is used to determine the smooth curve $\bar{\epsilon}(n)$. Shell-correction methods that are not based upon Eq. (4) and that consequently belong to a broader category have also been studied.[41, 110, 118-123] The primary advantage of Strutinsky's method is that it can be used for arbitrary distributions of single-particle energies that arise from realistic potentials of general shape, whereas up to now the other proposals cannot.

In Strutinsky's method the quantity that is given explicitly is the inverse of the function $\bar{\epsilon}(n)$, namely, the average particle number $\bar{n}(\epsilon)$ as a function of the single-particle energy. This quantity is determined by first noting that the *exact* particle number is given by

$$n(\epsilon) = \int_{-\infty}^{\epsilon} \frac{dn(\epsilon')}{d\epsilon'} d\epsilon' = \int_{-\infty}^{\epsilon} g(\epsilon')d\epsilon' \ ,$$

where the exact single-particle level density is

$$g(\epsilon) = \sum_{n=1}^{\infty} \delta(\epsilon - \epsilon_n) \ . \tag{5}$$

[Note that n is increased by 1 for each *particle*. This definition of $g(\epsilon)$ is the same as that used in studies of nuclear level densities,[124-126] and facilitates the discussion for an odd number of particles. However, in most other discussions of

Strutinsky's method, the quantity denoted by the same symbol is $\frac{1}{2}$ our $g(\epsilon)$.]

In principle the summation in Eq. (5) should extend over only the bound states, with the continuum states represented by an appropriate continuous expression. However, since the continuum states affect the final shell correction only in determining the smooth curve $\bar{\epsilon}(n)$ for particle numbers n at and below the Fermi surface, for this purpose they can be approximated with sufficient accuracy in terms of discrete states.

The next step is to separate the exact level density $g(\epsilon)$ into a smoothly varying part $\bar{g}(\epsilon)$ and a part $\delta g(\epsilon)$ that contains the local fluctuations, i.e.,

$$g(\epsilon)=\bar{g}(\epsilon)+\delta g(\epsilon)\,.$$

This is accomplished by expanding the δ function in a series of Hermite polynomials and then separating the terms into a smoothly varying part and a fluctuating part. This expansion includes automatically a Gaussian weighting function and leads to[115]

$$g(\epsilon)=\frac{1}{\gamma}\sum_{n=1}^{\infty}\delta(u_n)=\frac{1}{\gamma\sqrt{\pi}}\sum_{n=1}^{\infty}e^{-u_n^2}\sum_{m=0}^{\infty}c_m H_m(u_n)\,, \tag{6}$$

where we use the abbreviation

$$u_n=(\epsilon-\epsilon_n)/\gamma\,,$$

and where the coefficients c_m are given by

$$c_m=\begin{cases}\dfrac{(-1)^{m/2}}{2^m(m/2)!}\,, & m \text{ even}\\ 0\,, & m \text{ odd}\end{cases}$$

A scaling factor γ, which has the dimensions of energy, has been introduced to make the arguments dimensionless and to control the range over which the Gaussian weighting function is effectively nonzero. The summation over m in practice includes even values only, since the coefficients of all the odd Hermite polynomials are zero.

Since Hermite polynomials of low order oscillate more slowly than those of high order, the first few Hermite polynomials in Eq. (6) represent the smoothly varying contribution to $g(\epsilon)$, and the remaining terms the fluctuating contribution. Therefore, the smooth level density $\bar{g}(\epsilon)$ is given by an expression analogous to Eq. (6), but with the summation over m extending only to p (which defines the *order* of the shell correction) rather than to infinity. In the remaining fluctuating part $\delta g(\epsilon)$, the m summation runs from $p+1$ to infinity.

[The oscillations in the Hermite polynomials lead to a somewhat unpleasant feature of Strutinsky's method. In the process of decreasing to zero below the bottom level, the smooth level density $\bar{g}(\epsilon)$ in general becomes slightly negative for certain energies. This in turn causes the average particle number $\bar{n}(\epsilon)$ to also become slightly negative for certain energies below the bottom level. Therefore, the various integrals over particle number n in this subsection should in principle start at $-\infty$ rather than 0 when Strutinsky's method is used.]

The average particle number can now be evaluated explicitly to give

$$\bar{n}(\epsilon)=\int_{-\infty}^{\epsilon}\bar{g}(\epsilon')d\epsilon'$$
$$=\sum_{n=1}^{\infty}\left\{\tfrac{1}{2}[1+\mathrm{erf}(u_n)]-\frac{1}{\sqrt{\pi}}e^{-u_n^2}\sum_{m=1}^{p}c_m H_{m-1}(u_n)\right\}. \tag{7}$$

Conceptually, the next step is to invert this equation to give the average single-particle energy $\bar{\epsilon}(n)$ as a function of particle number. This function could then be inserted into Eq. (4) and the resulting integral evaluated numerically to give the shell correction.

However, in practice it is more convenient to transform the integration over particle number in Eq. (4) into an integration over energy, namely

$$\int_0^N\bar{\epsilon}(n)dn=\int_{-\infty}^{\bar{\lambda}}\epsilon\bar{g}(\epsilon)d\epsilon\,.$$

The upper limit $\bar{\lambda}$, which can be interpreted as the Fermi energy of the smooth distribution of levels, is illustrated in Fig 6. It is determined implicitly by the equation

$$\bar{n}(\bar{\lambda})=N\,,$$

which in practice is solved iteratively, with $\bar{n}(\bar{\lambda})$ given by Eq. (7). The desired integral can then be evaluated explicitly to give

$$\int_0^N\bar{\epsilon}(n)dn=\sum_{n=1}^{\infty}\left\{\tfrac{1}{2}\epsilon_n[1+\mathrm{erf}(\bar{u}_n)]-\frac{1}{2\sqrt{\pi}}\gamma e^{-\bar{u}_n^2}\right.$$
$$-\frac{1}{\sqrt{\pi}}e^{-\bar{u}_n^2}\sum_{m=1}^{p}c_m\left[\tfrac{1}{2}\gamma H_m(\bar{u}_n)\right.$$
$$\left.\left.+\epsilon_n H_{m-1}(\bar{u}_n)+m\gamma H_{m-2}(\bar{u}_n)\right]\right\}, \tag{8}$$

where we use the abbreviation

$$\bar{u}_n=(\bar{\lambda}-\epsilon_n)/\gamma\,.$$

Substitution of this result into Eq. (4) gives finally the shell correction.

As seen from Eq. (4) and Fig. 6, the shell correction depends explicitly upon the single-particle energies ϵ_n and the smooth curve $\bar{\epsilon}(n)$ only *below*

the Fermi surface $\bar{\lambda}$. Single-particle states above the Fermi surface enter implicitly only in determining the smooth curve $\bar{\epsilon}(n)$ for $n \leq N$, and the contributions of the higher states in determining this rapidly approach zero. In particular, in Eqs. (7) and (8) a given term n approaches zero as the energy ϵ_n exceeds the smooth Fermi energy $\bar{\lambda}$ by an amount that is large compared to the smoothing range γ. This means that the summations over n in these equations can be truncated as soon as $(\epsilon_n - \bar{\lambda})/\gamma \gg 1$.

Since neither the smoothing range γ nor the order p of the shell correction represent physical quantities, the value of the shell correction should be insensitive to these quantities as long as they are chosen suitably. Since the smooth curve $\bar{\epsilon}(n)$ is determined primarily by the single-particle levels within an interval γ to either side of $\bar{\epsilon}$, the value of γ should be large compared to the single-particle spacing, and in particular should be large enough to average over the levels between major shells. However, the value of γ should not be too large, because then levels far from the Fermi surface (in particular continuum states) would strongly affect the value of the shell correction. For the calculations reported here we have used the value $\gamma = 1.0\hbar\omega_0 = 41\ \mathrm{MeV}/A^{1/3}$ in a sixth-order correction ($p = 6$).

In Appendix B we discuss in greater detail the numerical accuracy of the shell correction calculated in this way. In addition to its dependence upon γ and p, we also examine the role played by the continuum states.[127,128] The conclusion is that for a given single-particle potential the shell correction can be calculated with a numerical accuracy of about 0.5 MeV, except for light nuclei, where the accuracy is less.

C. Pairing Correction

The second type of single-particle correction, the pairing correction, arises from the short-range interaction of correlated pairs of nucleons moving in time-reversed orbits. This is the most important and easily treated of the many residual interactions felt by a nucleon. This interaction always lowers the total potential energy relative to the energy without pairing. However, relative to the pairing energy of a smooth distribution of levels representing an "average" nucleus, the pairing correction can have either sign. The lowering in energy is larger when more pairs of nucleons are able to interact, which occurs when the level density near the Fermi surface is high. This is opposite to the behavior of the shell correction, where the potential energy is lowered most when the level density is low. This leads to a partial cancellation of effects between the shell and pairing corrections. The shell correction is the larger of the two, and therefore the main trends of the total single-particle correction are determined by the shell correction.

The essential features of the pairing correction can be described in terms of a *constant* pairing interaction G acting between a given number of pairs of particles.[129] Then a standard pairing calculation in the BCS approximation tells how much the energy is lowered for the actual distribution of levels. A similar calculation performed for the same number of particles distributed smoothly according to $\bar{\epsilon}(n)$ (or in practice distributed uniformly) determines the lowering in energy for an average nucleus. The difference between the lowering for the actual levels and the lowering for the smooth levels gives the pairing correction.

In calculating the pairing correction for either neutrons or protons, we consider N_p pairs of particles, with $\frac{1}{2}N_p$ pairs lying above the sharp Fermi surface and $\frac{1}{2}N_p$ pairs lying below. (Our discussion of the pairing correction is limited to the case of even particle numbers; some aspects of odd-particle effects are discussed in Refs. 44 and 51.) Then, for a specified pairing strength G, the pairing correlation energy (relative to the energy without pairing) is given in the BCS approximation by[90,129]

$$E_{\mathrm{pc}} = 2\left(\sum_{k=1}^{N_p} \epsilon_k v_k^2 - \sum_{k=1}^{\frac{1}{2}N_p} \epsilon_k\right) - \frac{\Delta^2}{G} - G\left(\sum_{k=1}^{N_p} v_k^4 - \sum_{k=1}^{\frac{1}{2}N_p} 1\right) . \tag{9}$$

[To conform to standard pairing theory notation, the summations in this discussion are over the *pairs* of particles considered in the pairing interaction rather than over the single particles themselves. Note that Eq. (9) gives the pairing *correlation* energy,[40] which is shifted by the constant amount $\frac{1}{2}GN_p$ relative to the energy considered in most pairing discussions. Since this same constant term is also present in the *average* pairing correlation energy, the final pairing correction is completely independent of whether or not it is included.]

With the further standard approximation that the variation of the v_k^4 term in Eq. (9) is neglected, the pairing gap Δ and the BCS Fermi energy λ (which we do not need explicitly) are given by the solutions of the equations

$$N_p = \sum_{k=1}^{N_p} \left\{ 1 - \frac{\epsilon_k - \lambda}{[(\epsilon_k - \lambda)^2 + \Delta^2]^{1/2}} \right\} , \tag{10}$$

and

$$\frac{2}{G} = \sum_{k=1}^{N_p} \frac{1}{[(\epsilon_k - \lambda)^2 + \Delta^2]^{1/2}} . \tag{11}$$

The occupation probabilities appearing in Eq. (9) are given by

$$v_k^2 = \tfrac{1}{2}\left\{1 - \frac{\epsilon_k - \lambda}{[(\epsilon_k - \lambda)^2 + \Delta^2]^{1/2}}\right\}, \quad k = 1, 2, \ldots, N_p . \tag{12}$$

The pairing correlation energy of an average nucleus is determined from expressions analogous to Eqs. (9)–(12), but with the summations over discrete states ϵ_k replaced by integrals over the smooth function $\bar{\epsilon}(n)$ of Fig. 6. The resulting integrals can be evaluated explicitly if $\bar{\epsilon}(n)$ is replaced by a linear function (obtained by making a Taylor expansion about the sharp-Fermi-surface particle number and neglecting terms quadratic and higher). The *inverse* of the slope of this curve is simply $\bar{g}(\bar{\lambda})$ and is obtained by means of the methods discussed in the last subsection. The average density of *pairs* is then given by

$$\bar{\rho} = \tfrac{1}{2}\bar{g}(\bar{\lambda}) .$$

For such a *uniform* distribution of levels, the pairing correlation energy is given explicitly by

$$\bar{E}_{pc} = -\frac{1}{4}\frac{N_p^2}{\bar{\rho}}\left\{\left[1 + \left(\frac{2\bar{\rho}\bar{\Delta}}{N_p}\right)^2\right]^{1/2} - 1\right\} + \tfrac{1}{2}\bar{\rho}\bar{\Delta}G\tan^{-1}\frac{N_p}{2\bar{\rho}\bar{\Delta}} ,$$

with the pairing strength G and the average pairing gap $\bar{\Delta}$ related by

$$\frac{1}{G} = \bar{\rho}\ln\left\{\left[\left(\frac{N_p}{2\bar{\rho}\bar{\Delta}}\right)^2 + 1\right]^{1/2} + \frac{N_p}{2\bar{\rho}\bar{\Delta}}\right\}. \tag{13}$$

The pairing correction for either neutrons or protons is given finally by

$$\Delta E_{pc} = E_{pc} - \bar{E}_{pc} .$$

This formulation of the pairing correction[11, 12, 30] permits the strengths G for neutrons and protons to be determined directly from the average behavior of odd-even mass differences. The value of G for either neutrons or protons is given by Eq. (13), with the average pairing gap $\bar{\Delta}$ chosen to reproduce exactly the semiempirical result

$$\bar{\Delta} = 12 \text{ MeV}/\sqrt{A}$$

for the average mass difference of neighboring nuclei that differ by one neutron or one proton.[130, 131]

The value of $\bar{\Delta}$ is assumed to remain constant with deformation. This is motivated by the lack of any direct evidence, either experimental or theoretical, for the pairing strength depending upon deformation. Several years ago some interpretations of fission-fragment angular-distribution data suggested that the pairing gap is a strong function of deformation,[132, 133] but these conclusions are now in doubt,[134–136] because the analyses did not take into account the presence of two peaks in the fission barrier. The available theoretical studies[137] of the shape dependence of the pairing strength are also inconclusive.

When $\bar{\Delta}$ is taken to be the independent parameter describing the pairing interaction, the logarithmic dependence of the strength G upon the number of pairs considered is taken into account automatically.[11, 12, 30] It is not necessary to make the usual artificial prescriptions[31–67] relating the pairing strength and number of pairs in order to reproduce approximately the desired average odd-even mass difference.

For most of our calculations we have taken into account all *bound* levels above the Fermi surface and an equal number below, or all levels below the Fermi surface and an equal number above if there are fewer levels below than above. (However, in calculating the results to be shown later in Fig. 17, we have for $Z > 114$ included proton levels up to an energy of 5 MeV rather than 0, as well as an equal number below the Fermi surface.) Since for a given number of pairs the strength G is determined to reproduce exactly the desired average pairing gap $\bar{\Delta}$, the final pairing correction depends upon N_p only very weakly. This point is discussed more thoroughly in Appendix B, where it is concluded that for a given single-particle potential and value of $\bar{\Delta}$, the pairing correction can be calculated with a numerical accuracy of about 0.1 MeV, except for light nuclei, where the accuracy is less.

VI. CALCULATED FISSION BARRIERS

In this section we present a limited selection of results for heavy and superheavy nuclei that have been obtained thus far. These represent only a few of the many possible applications that we plan to make. In particular, one of the more important applications is the calculation of ground-state single-particle corrections for use in nuclear mass formulas. Our preliminary results on these corrections indicate that the over-all trends of experimental ground-state single-particle corrections are reproduced by the calculations, but that the magnitude of the calculated corrections is somewhat too large. A similar conclusion is reached in Ref. 30. We have not made a detailed comparison, since we have not yet allowed for the possibility of positive hexadecapole (diamond-like) deformations. The inclusion of these deformations lowers the ground-state single-particle correction for some heavy deformed nuclei[30, 40] by as much as about 2 MeV. We therefore postpone presenting such results until positive hexadecapole deformations have been taken into account.

A. Heavy Nuclei

The dependence of the single-particle energies upon the approximate fission coordinate y is shown in Figs. 7 and 8 for, respectively, the neutrons and protons in ^{240}Pu. For the spherical shape the usual gaps are observed in the single-particle levels at 82, 126, and 184 neutrons and at 50, 82, and 114 protons. Fairly large gaps associated with secondary shells also occur for 150 neutrons at $y \approx 0.07$, for 142 neutrons at $y \approx 0.16$, and for 146 neutrons at $y \approx 0.18$, as well as for 98 protons at $y \approx 0.07$ and for 100 protons at $y \approx 0.08$. Such secondary shell structure is responsible for the occurrence of deformed ground-states and secondary minima in the fission barriers of nuclei containing approximately these numbers of nucleons.

The quantum numbers shown in the figures for the deformed states give the parity and the projection Ω (or K) of the particle's total angular momentum on the nuclear symmetry axis. In addition, states of even parity are drawn as solid curves, and states of odd parity as dashed curves. It is observed that states having the same quantum numbers (Ω and parity) do not cross, in accordance with the von Neumann-Wigner noncrossing rule.[138-141]

At the deformation $y \approx 0.3$, the lower levels for each value of Ω begin to group into nearly degenerate pairs of levels with opposite parity. The

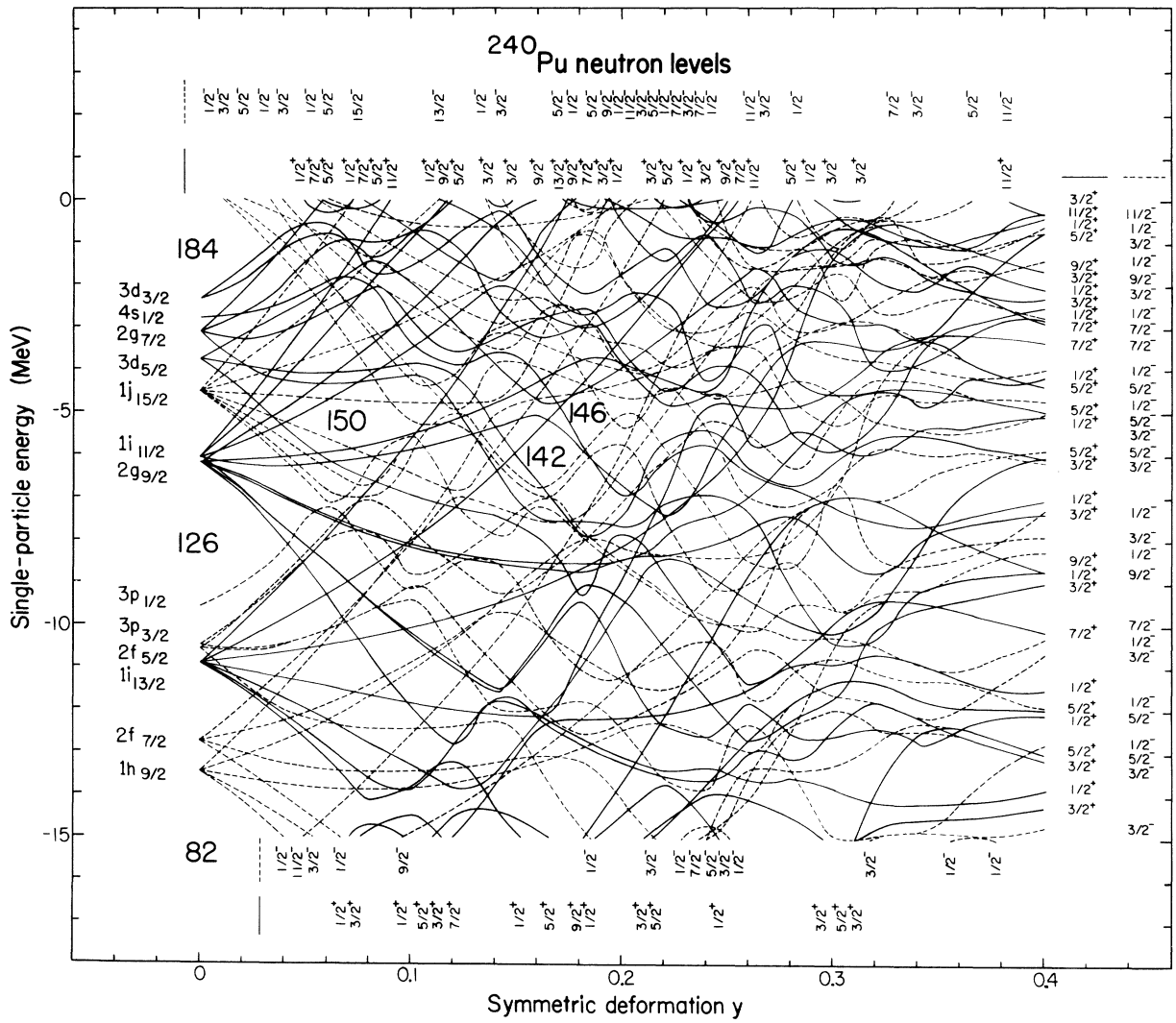

FIG. 7. Single-neutron energies near the Fermi surface of ^{240}Pu as a function of the symmetric-deformation coordinate y. The levels are labeled by the parity and the projection Ω (or K) of the total angular momentum on the nuclear symmetry axis. In addition, odd-parity levels are drawn dashed. The quantum numbers for the spherical levels are shown at the left. States up to $N_0 = 14$ are included in the harmonic-oscillator basis (see Sec. IV).

primary reason is that at this deformation the nucleus begins to develop a neck, which both raises the potential slightly and reduces its volume in the neck region. This means that an even-parity wave function will nearly vanish in the neck and consequently will have almost the same energy as the corresponding odd-parity solution. This implies that the particles begin to feel the formation of the fragments at a very early stage in the division process, a conclusion that has also been reached in Refs. 60–62, 68, and 78. For reflection-asymmetric shapes these near degeneracies are of course broken.

In Fig. 9 we show the dependence of the potential energy on the approximate fission coordinate y for a group of actinide nuclei differing from each other by four protons and four neutrons. The positions of the nuclei correspond to those in a chart of the nuclides, with the rows representing proton numbers 90, 94, 98, and 102 and the columns neutron numbers 142, 146, 150, and 154. The dashed curves give the liquid-drop contributions and the solid curves the total potential energies.

These results are qualitatively similar to those of several previous calculations; see for example Refs. 30, 40, 62, and 63. Each nucleus is seen to have both a deformed ground-state minimum and also a secondary minimum. The calculated quadrupole moments of the ground-state minima are in approximate agreement with experimental values.[142]

Relative to the spherical liquid-drop energy, the values of the secondary minimum and the two peaks increase as neutrons are added up to neu-

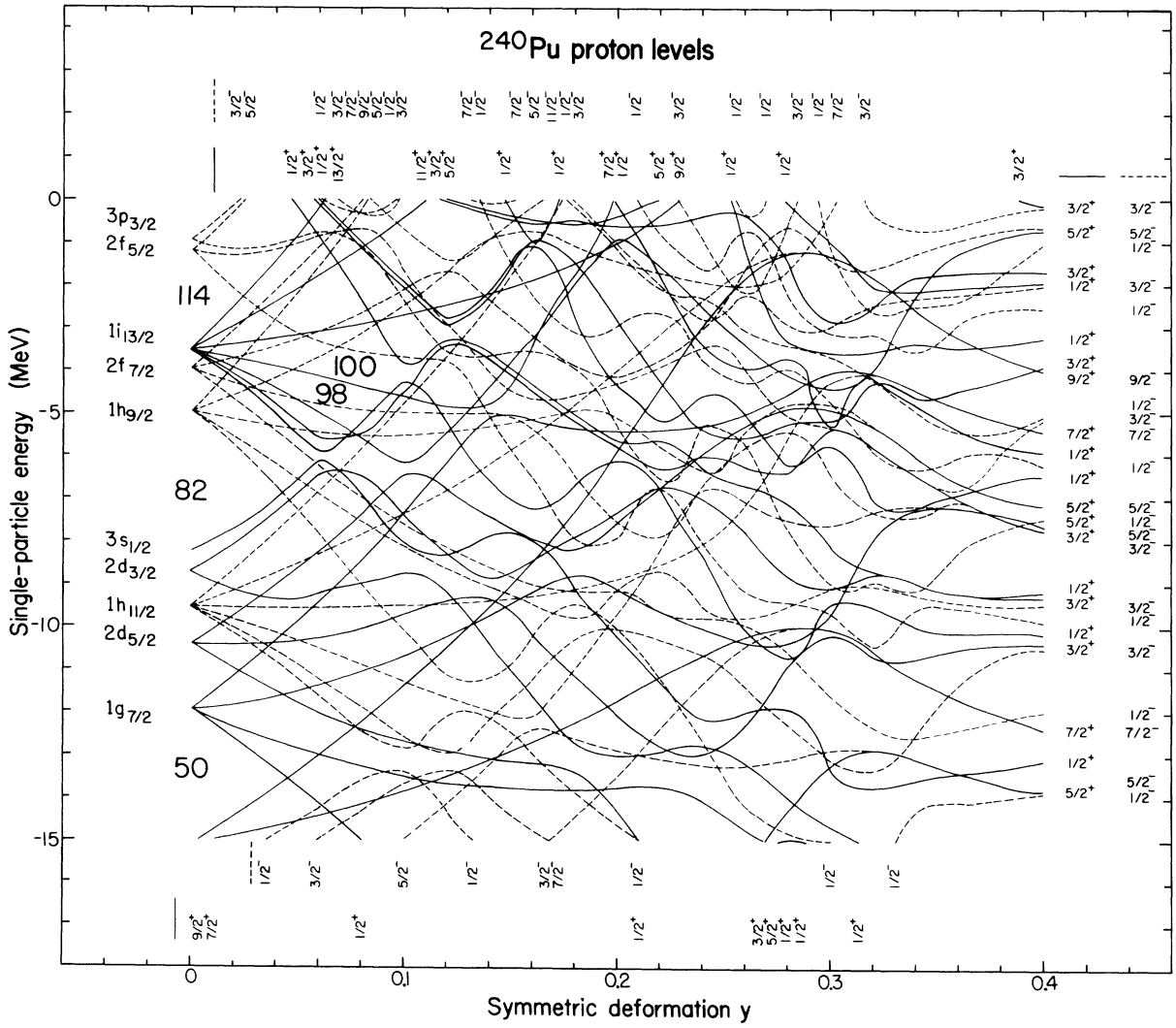

FIG. 8. Single-proton level diagram, analogous to Fig. 7.

tron number $N \approx 152$, and then decrease gradually. The ground-state minimum initially decreases with the addition of neutrons, but part of the decrease evident in the figure is a spurious effect associated with our restriction to shapes described by the coordinate y. This family of shapes contains a small indentation at the equator (relative to spheroidal shapes), whereas the true ground-state shapes of the lighter actinide nuclei prefer a small bulge, that is, they prefer a positive hexadecapole (diamond-like) deformation. For example, for ^{240}Pu the ground-state energy shown in the figure is lowered by 0.7 MeV when *spheroidal* deformations are introduced, and by about an additional[30] 0.6 MeV, for a total of about 1.3 MeV, when positive hexadecapole deformations are introduced. Since the magnitude of the hexadecapole deformation increases with decreasing neutron number,[40] the calculated ground-state energy is raised more by our shape restriction for nuclei having a smaller number of neutrons (such as ^{232}Th and ^{236}Pu). Therefore, the calculated heights of the secondary minimum and the two peaks relative to the ground-state energy increase somewhat less rapidly with the addition of neutrons than is implied by the figure.

Whereas the variation of the potential energy with neutron number arises primarily from single-particle effects, its variation with proton number is associated also with large changes in the liquid-drop energy. Increasing the proton number Z increases the fissility parameter x, which pulls in the maximum of the liquid-drop energy to make the first peak higher than the second. Conversely, decreasing Z decreases x, which pushes out the liquid-drop maximum to make the second peak higher than the first.

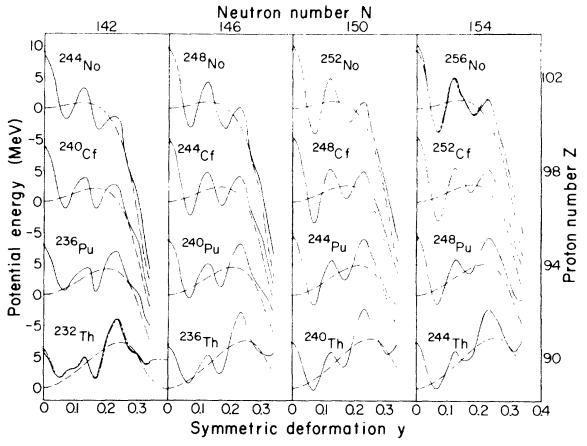

FIG. 9. Dependence of potential energy of actinide nuclei upon the symmetric-deformation coordinate y. The dashed curves give the liquid-drop contributions and the solid curves the total potential energies, which are calculated with single-particle levels for ^{240}Pu. The dot-dashed curve for ^{232}Th is calculated with single-particle levels for ^{226}Ra, and the dot-dashed curve for ^{256}No with levels for ^{258}Fm. The solid points at zero deformation are calculated with the appropriate spherical single-particle levels for each individual nucleus.

These fission barriers have all been calculated using single-particle levels for the nucleus ^{240}Pu. This represents a numerical approximation, because the levels themselves are somewhat different for the different nuclei. An idea of the accuracy of this approximation is gained by comparing the curves at zero deformation with the solid points, which have been calculated using spherical levels appropriate to the particular nucleus. In addition, the dot-dashed curve for ^{232}Th has been calculated from single-particle levels for ^{226}Ra, and the dot-dashed curve for ^{256}No from levels for ^{258}Fm. The approximation is fairly good for nuclei close to the nucleus for which the levels have been calculated, but grows worse for nuclei far away. The reason it works fairly well is because the shell and pairing corrections depend mainly upon the *spacings* between the levels near the Fermi surface, and the spacings remain nearly constant with changes in N and Z, even though the actual positions of the levels change by relatively large amounts. Since the dot-dashed curves for ^{232}Th and ^{256}No lie neither entirely above nor entirely below the corresponding solid curves, it is *not* possible when using realistic diffuse surface potentials to correct for the use of different single-particle levels by simply scaling the results by a geometric factor, as is sometimes done.[30]

In addition to the symmetric fission coordinate, it is also important to examine how the potential energy depends upon the remaining coordinates, especially the mass-asymmetry coordinate. From simple qualitative considerations, one expects that when the nucleus encounters a high and sharp peak in the total potential energy as a function of the symmetric fission coordinate, it would be energetically favorable to go *around* rather than over the peak by taking advantage of asymmetric deformations. This expectation stems from the observation that single-particle corrections *oscillate* about an average of zero, and that if one is already at a high and sharp peak in the fission coordinate, the single-particle correction is expected to decrease also for asymmetric deformations. Then, provided that the liquid-drop energy does not increase too rapidly, the total potential energy should have an asymmetric path of lower energy leading around the symmetric peak.[143] Conversely, a deep minimum in the single-particle correction as a function of the symmetric fission coordinate is expected to lead to increased stability with respect to

asymmetric deformations.

The upper part of Fig. 10 shows again the calculated dependence of the potential energy of ^{240}Pu on the symmetric coordinate y. From our qualitative discussion we would expect the potential energy to be stable with respect to mass asymmetry at both the first and second minima, and this turns out to be the case. At the first minimum, the potential energy is actually lowered somewhat when the two remaining *symmetric* coordinates are considered. This is because the ground-state shape of ^{240}Pu prefers a small bulge at the equator rather than the indentation that is present in the coordinate y. The arrow at the first minimum indicates the amount the potential energy is lowered when the shapes are permitted to become *spheroidal*; the inclusion of positive hexadecapole (diamond-like) shapes would lower the ground-state energy

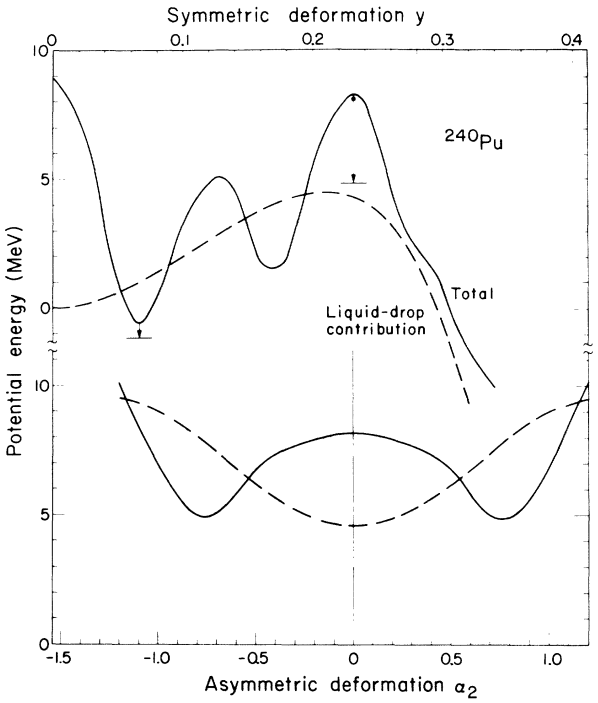

FIG. 10. Dependence of potential energy (solid curves) of ^{240}Pu upon the approximate fission coordinate y (top) and mass-asymmetry coordinate α_2 (bottom). The dashed curves give the liquid-drop contribution. The arrow at the ground-state minimum indicates the amount the potential energy is lowered when spheroidal deformations are included. At the second peak the solid point indicates the amount the potential energy is lowered when the remaining two symmetric coordinates are included, and the arrow the further lowering associated with the asymmetric coordinate α_2. In the lower part of the figure, the three symmetric coordinates are held fixed at their values corresponding to the second symmetric saddle point (whose energy is given by the solid point).

by about an additional[30] 0.6 MeV. At other deformations the coordinate y was found to be more satisfactory; for example, at the second peak the introduction of the other two symmetric coordinates lowers the energy by only the small amount indicated by the solid point.

The second peak extends well above the liquid-drop background, by an amount roughly twice that of the first peak. In accordance with our qualitative expectations, the second peak is indeed found to be unstable with respect to mass asymmetry, as shown in the lower part of Fig. 10. This part of the figure shows how the potential energy varies with the mass-asymmetry coordinate α_2, for fixed values of the symmetric coordinates corresponding to the second symmetric saddle point (whose energy is given by the solid point). The coordinate α_2 is defined by[75]

$$\alpha_2 = \frac{a_1^2 - a_2^2}{\frac{1}{2}(a_1^2 + a_2^2)} ,$$

where a_1 and a_2 are the transverse semiaxes of, respectively, the left-hand and right-hand spheroids forming the shape, as illustrated in Fig. 3. Strictly speaking, the mass-asymmetry coordinate should contain a small component of the asymmetric coordinate α_3 (defined in Ref. 75), but this was found to be extremely small and is consequently neglected. (The coordinates α_2 and α_3 used here should not be confused with the Legendre-polynomial expansion coefficients usually designated by the same symbols.) Also, we neglect here the possible changes in the symmetric coordinates that occur between the symmetric peak and the asymmetric saddle point. With these approximations, the potential energy of the asymmetric saddle point is 3.2 MeV lower than the energy of the symmetric saddle point. As indicated by the arrow at the second peak, the inclusion of the mass-asymmetry degree of freedom reduces the height of the second saddle point to slightly below that of the first. The first peak, which extends above the liquid-drop energy by a smaller amount than the second peak, is found to be stable with respect to mass asymmetry.

Results qualitatively similar to these were first obtained by Möller and Nilsson with a generalized deformed harmonic-oscillator potential[49] and have also been confirmed with more realistic potentials.[27-30] Since the single-particle corrections are correlated with the distribution of single-particle levels near the Fermi surface, the level density is lower than average at the two minima *and at the asymmetric saddle point,* and is higher than average at the first saddle.

The calculated shapes of the equilibrium points for ^{240}Pu are shown in Fig. 11. The ground-state

minimum, first saddle, and second minimum are symmetric in shape, but the second saddle has the asymmetric shape shown by the solid curve. The dashed curve gives the corresponding shape for the symmetric peak.

Figure 12 shows the calculated liquid-drop and total potential energies vs the symmetric deformation coordinate y for the lighter nucleus ^{210}Po. Because it is near a doubly closed shell, ^{210}Po has a large negative spherical shell correction, which increases the barrier height considerably. The second minimum in this barrier should lead to a shape-isomeric state that would decay primarily back to the ground state by γ emission. For values of y approaching 0.4 this coordinate ceases to represent motion in the fission direction,[98] and the rise in both the liquid-drop and total energies on the right-hand side of the graph should be disregarded. Unlike Möller and Nilsson[49] and Pauli *et al.*,[27] we find that ^{210}Po is slightly *unstable* with respect to mass asymmetry at its highest symmetric peak, which extends well above the liquid-drop energy. However, for values of y slightly beyond the highest symmetric peak the total potential energy drops well below the liquid-drop energy, which suggests that the dynamical path for this nucleus would possibly revert to symmetric shapes after passing over the asymmetric saddle point.

Figure 13 shows a similar calculation for the still lighter nucleus ^{188}Os. Since this nucleus is deformed in its ground state, the barrier height is determined mainly by the liquid-drop contribution. Although the total barrier oscillates several times, there is no suggestion of a local minimum sufficiently deep to form a shape-isomeric state. This nucleus is found to be stable with respect to mass asymmetry at the highest peak, which was expected, since the total potential energy does not extend above the liquid-drop energy at this point.

The stability of the potential energy with respect to mass asymmetry was also considered for the nuclei ^{226}Ra and ^{258}Fm. We found that the highest saddle point for ^{226}Ra is asymmetric in shape and 2.3 MeV lower in energy than the corresponding symmetric peak. There is *no* indication of both symmetric and asymmetric saddle points of comparable energy. The second saddle point for ^{258}Fm is asymmetric and 2.0 MeV lower in energy than the second symmetric peak. The second minimum has almost vanished, since its energy is approximately the same as that of the asymmetric saddle point. As in other actinide nuclei, the first saddle point for ^{258}Fm is symmetric.

We have not attempted at this stage a comprehen-

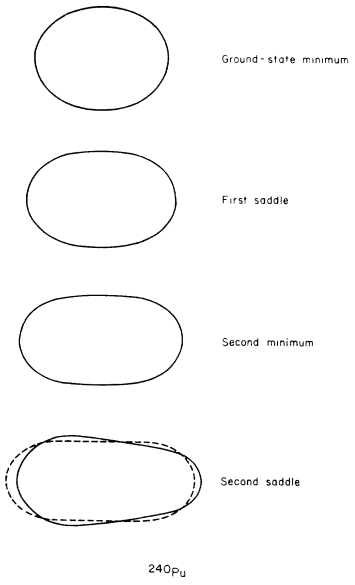

FIG. 11. Calculated equilibrium shapes for ^{240}Pu. At the second saddle the solid curve gives the shape of the asymmetric saddle point, and the dashed curve the corresponding shape for the symmetric peak.

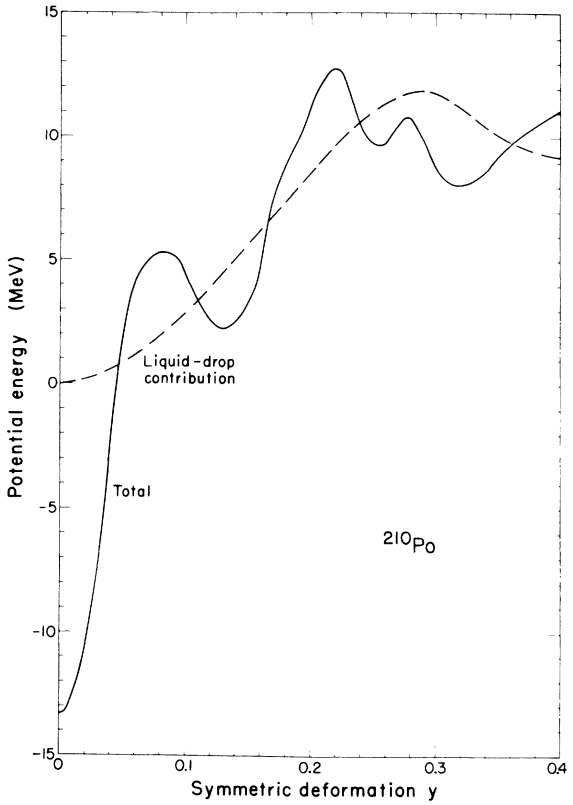

FIG. 12. Dependence of potential energy of ^{210}Po upon the symmetric deformation coordinate y.

sive comparison of our calculations with experimental results. Nevertheless, some important conclusions can be drawn even from a limited comparison.

First, we have seen that single-particle effects lead to secondary minima in the calculated fission barriers of actinide nuclei. Evidence for such secondary minima is available experimentally from three sources: (1) spontaneously fissioning isomeric states, (2) broad resonances in fission cross sections, and (3) narrow intermediate structure in fission cross sections.[16, 23-26, 144] These phenomena have now been observed in a variety of actinide nuclei for which the calculations indicate fairly deep secondary minima; conversely, they have not been seen in nuclei for which the calculated barriers have shallow secondary minima or none at all. Thus, the calculations describe correctly the general region of nuclei that contain deep secondary minima.

Second, experimental information on the heights of the first and second saddles and the secondary minimum is now becoming available for some nuclei. Table I compares the experimental results of Britt *et al.*[145] for ^{240}Pu with the calculated heights, which are relative to a ground-state energy calculated for *spheroidal* shapes. As mentioned earlier, the inclusion of positive hexadecapole (diamond-like) deformations would lower the ground-state energy by about 0.6 MeV and hence increase each of the three calculated heights by this constant amount. Since for spheroidal ground-state shapes the calculations reproduce the experimental heights to within 0.25 MeV, the inclusion of hexadecapole deformations would result in calculated heights that are somewhat larger than the experimental heights. This possibly indicates that the ratio of the surface energy to Coulomb energy should be slightly smaller for actinide nuclei than that given by the Lysekil conference Myers-Swiatecki nuclear mass formula[4] which we are using. This same conclusion has also been reached by Pauli and Ledergerber.[28]

TABLE I. Comparison of experimental and calculated fission-barrier heights.

Nucleus		Experimental height (MeV)	Calculated height (MeV)
^{240}Pu	First saddle	5.8 [a]	5.8 [b]
	Second minimum	2.6 [a]	2.7 [b]
	Second saddle	5.35 [a]	5.6 [b]
^{210}Po		20.4 [c]	<24.1 [d]
^{188}Os		23.7 [e]	21.3

[a] Reference 145.
[b] Relative to a ground-state energy calculated for spheroidal shapes.
[c] References 111 and 146.
[d] The inequality arises because this nucleus is calculated to be unstable with respect to mass asymmetry at its highest peak, whereas the exact energy of the asymmetric saddle point has not yet been determined.
[e] References 111 and 147.

Similar comparisons for other actinide nuclei show that the calculations reproduce approximately the over-all dependence upon proton number of the heights of the first and second saddles and the secondary minimum. However, the calculated heights of the first peaks are somewhat lower than the experimental values for thorium isotopes and somewhat higher for curium isotopes; these discrepancies have also been observed by Pauli and Ledergerber.[28] The calculated heights of the second minimum show a greater variation with neutron number than the experimental heights (even after estimates are made of the influence of positive hexadecapole deformations on the ground-state energy).

Table I also includes the experimental[111, 146, 147] and calculated barrier heights for ^{210}Po and ^{188}Os. The calculated height for ^{210}Po is larger than the

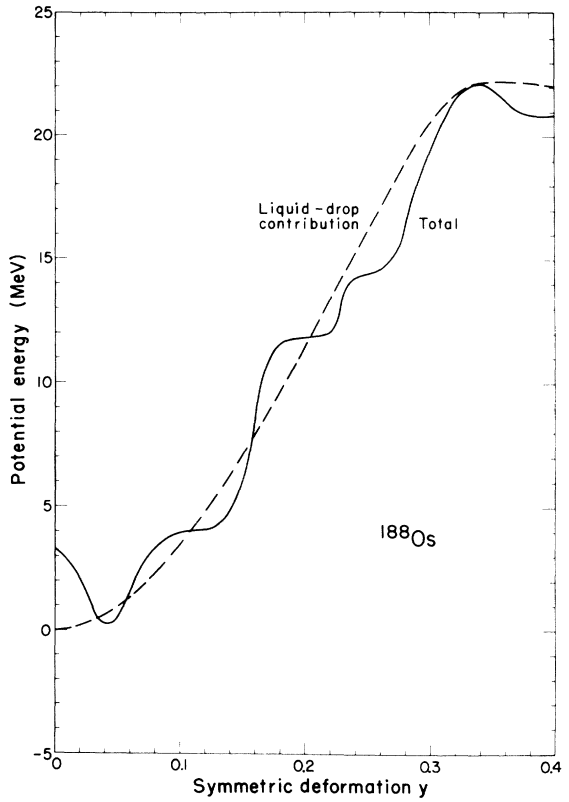

FIG. 13. Dependence of potential energy of ^{188}Os upon the symmetric deformation coordinate y.

experimental height by some 10 to 15% and for ^{188}Os is smaller by about 10%. It should be stressed that in all these comparisons no arbitrary parameters have been adjusted; the experimental and calculated results have not been normalized to one another in any way. (For each nucleus in Table I we have taken 0.5 MeV as an estimate of the zero-point energy in the fission degree of freedom at the ground-state minimum and secondary minimum.[53, 148, 149])

Finally, we would like to discuss in a qualitative way the extent to which experimental fission-fragment mass distributions can be understood in terms of the calculated properties of the saddle points. Most of the experimental information on mass distributions that we want to consider has been known for a long time[150]: At low excitation energies, heavy nuclei ($Z \geq 90$) divide primarily into one large and one small fragment. As the excitation energy increases, the probability for division into two equal fragments increases, until at high energies the mass distribution is peaked about a division into two equal fragments. The mass distributions for nuclei in the vicinity of radium ($84 < Z < 90$) have *three* peaks, one corresponding to division into equal fragments and the others to division into unequal fragments. Increasing the excitation energy increases the probability for an equal-mass division. Still lighter nuclei like Po ($Z \leq 84$) divide primarily into two equal fragments at all excitation energies for which the mass distributions are known. More recent experiments[151, 152] have shown that the degree of mass asymmetry also decreases strongly for very heavy nuclei. In particular, the most probable mass split in the thermal-neutron-induced fission of ^{257}Fm ($Z = 100$) is symmetric.[152]

To what extent are single-particle effects able to account for these experimental observations, namely, the mass asymmetry in the low-energy fission of actinide nuclei, the three-peaked mass distributions for radium, and the transitions to symmetric divisions for both lighter and heavier nuclei and at high excitation energies?

We have seen that for unexcited actinide nuclei the second saddle points are calculated to be asymmetric in shape. At low energies an actinide nucleus will therefore start its descent from the saddle point to scission in an asymmetric shape. But it is a fairly long way to scission – some 40-MeV decrease in potential energy and a complete development and constriction of a neck – and the saddle asymmetry could be destroyed en route. On the other hand, the potential energy drops rapidly beyond the second saddle, and the inertia associated with a rapid descent of the nucleus could override subsequent forces that would prefer an equal-mass division. In this case an asymmetric mass division would result, in accordance with the experimental observations.

The saddle points of light nuclei like ^{188}Os are calculated to be symmetric in shape, which could be responsible for the transition to symmetric mass divisions in lighter nuclei. If we go the other way, for the heavier actinide nuclei the second saddles decrease in height relative to the first, and the nucleus begins its descent with a shape corresponding to the first saddle. But the shape at the first saddle is symmetric, which could explain the transition to symmetric divisions in the thermal-neutron-induced fission of ^{257}Fm.

The transition to symmetric divisions with increasing excitation energy is probably associated with the decrease in relative importance of single-particle effects at high excitation energies. At high excitations, the nucleons are distributed randomly over a large number of single-particle levels. This effectively destroys the influence of the shells, and, in a loose manner of speaking, the system divides in accordance with the smooth macroscopic contribution to the energy, which prefers an equal-mass split.

The phenomena that one is able to understand qualitatively in terms of the calculated saddle points are thus the mass asymmetry in the low-energy fission of actinide nuclei, and the transitions to symmetric divisions for both lighter and heavier nuclei and at high excitation energies. The calculated saddle points do not reproduce the

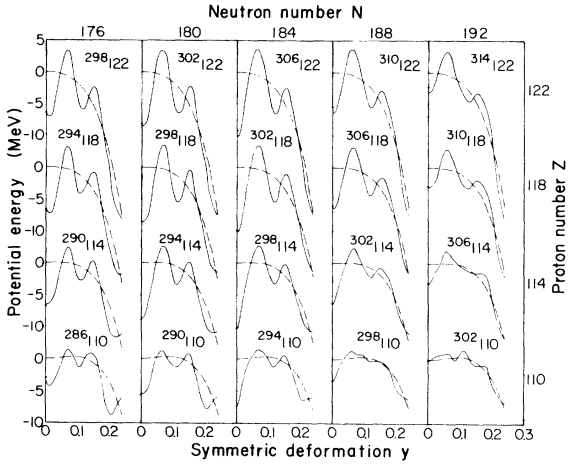

FIG. 14. Dependence of potential energy of superheavy nuclei upon the symmetric-deformation coordinate y. The dashed curves give the liquid-drop contributions and the solid curves the total potential energies, which are calculated with single-particle levels for ^{298}114. The solid points at zero deformation are calculated with the appropriate spherical single-particle levels for each individual nucleus.

exact location of the transition to symmetric divisions for lighter nuclei, and also do not reproduce the expected symmetric and asymmetric saddle points for nuclei like radium in the transition region.

On the other hand, it is still possible that the mass distribution could be altered somewhere beyond the saddle point during its dynamical descent to scission, or even be determined altogether somewhere close to the scission point. This point of view is made plausible by the dynamical calculations of Hasse,[153] which demonstrate that a single-particle correction of reasonable magnitude near scission can lead to a preference for asymmetric mass divisions, even for dynamical paths that start from approximately symmetric shapes. In addition, the potential energy surfaces calculated by Mosel and Schmitt[60-62] with a generalized two-center harmonic-oscillator potential suggest that single-particle effects can be very large near the scission point.

The calculations performed thus far have been somewhat fragmentary and have concentrated on the region near the saddle point. The next step is to examine systematically the region between saddle and scission for a wide range of nuclei. Ideally the kinetic energy should also be calculated and the equations of motion solved to give the actual dynamical paths. But a fair approximation to the dynamical paths might be obtained from maps of the potential energy vs fission and mass-asymmetry coordinates that have been selected previously in such a way as to minimize inertial effects. In this way one could possibly decide the important question of where, between saddle and scission, single-particle effects are most important in determining the mass distribution.

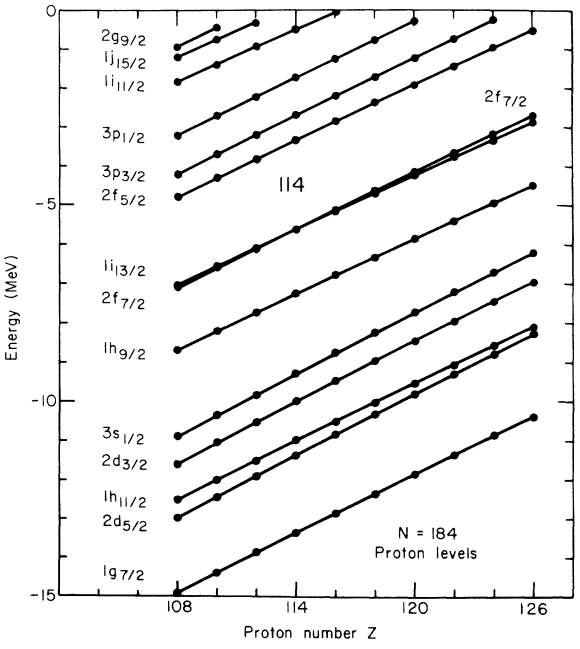

FIG. 15. Dependence of spherical proton levels upon proton number for superheavy nuclei containing 184 neutrons.

B. Superheavy Nuclei

Some of our results for superheavy nuclei have already been discussed in Refs. 68–70, but will be repeated here for completeness.

Figure 14 summarizes our calculated fission barriers for superheavy nuclei. The positions of the nuclei correspond to those in a chart of the nuclides, with the nuclei differing from each other by four neutrons and four protons. For the doubly-closed-shell nucleus $^{298}114$, the spherical single-particle correction is −10.3 MeV. As the nucleus deforms the total potential energy (solid curve) increases until it reaches a maximum value of 2.7 MeV at the deformation $y = 0.07$. Further deformation leads to a secondary minimum followed by a somewhat lower second peak. Beyond this peak the barrier drops rapidly. The difference in energy between the highest peak and the spherical shape is 13.0 MeV.

As neutrons are added beyond 184, the barrier height decreases drastically. Subtracting neutrons also lowers the barrier, but not as much as if the same number were added. When a small number of protons are added beyond 114, the barrier heights actually increase slightly. When protons are subtracted, the barrier is again lowered.

For the nuclei near the top of Fig. 14, the peaks extend well above the liquid-drop background, and it is possible that mass-asymmetric or axially asymmetric (γ) deformations could lower these barriers somewhat. However, the results of Refs. 51–53 and 74 suggest that the amount of this lowering is rather small. (Other results[154-156] would imply that superheavy nuclei undergo oblate fission through a barrier that is some 5 MeV lower than the barrier for prolate fission. However, we discount these results, since these barriers were calculated by simply summing single-particle energies, a procedure which is now known to be seriously inadequate.[148,157])

Figures 15 and 16 aid in understanding why the barrier heights depend upon neutron and proton numbers in the way they do. As seen in Fig. 15, the level density is very high for spherical nuclei containing a few protons less than 114, since 14 particles fill the $1i_{13/2}$ level and 8 fill the $2f_{7/2}$ level. The level density of spherical nuclei containing a few more protons than 114 is relatively lower, which explains why such nuclei continue to

have fairly high fission barriers.

As the proton number increases (with the neutron number held fixed at 184), the proton separation energy decreases substantially. In fact, when $Z \geq 126$ the Fermi surface lies in the continuum, which means that these nuclei are unstable with respect to proton emission. (Of course this mode of decay will be less rapid than α emission.)

As seen in Fig. 16, the neutron level density is lower when the number of neutrons is slightly less than 184, than when the number is slightly more. This explains why the barrier heights decrease more rapidly with the addition of neutrons beyond 184 than with their subtraction. We also see that for a fixed number of neutrons the neutron separation energy increases with increasing proton number. This of course makes it harder to emit neutrons, which is a handicap with respect to getting rid of excess excitation energy in attempts to produce superheavy nuclei.

Many of the points we have tried to make are conveniently summarized in Fig. 17, which is a contour map of the single-particle correction for spherical superheavy nuclei vs neutron and proton numbers. As we move away from the doubly-closed-shell nucleus with 114 protons and 184 neutrons, the spherical single-particle correction decreases in magnitude from −10 MeV for nuclei along the inner contour to −5 MeV for nuclei along the outer contour. The fission-barrier height decreases in a similar way. (These results are obtained from single-particle levels recomputed for each individual nucleus.) The portions of contour lines shown dashed correspond to nuclei calculated to be proton unstable. The dot-dashed curve gives the line of β stability, which has been determined by minimizing the calculated masses for even spherical nuclei with respect to $N-Z$ for constant mass numbers A.

The present fission barriers are somewhat higher than most of those calculated previously by means of the macroscopic-microscopic method, both for generalized harmonic-oscillator potentials[11-13, 19, 35-42, 46] and for diffuse-surface potentials.[13, 19, 67] The primary reason for this is that our present single-particle potential radius is somewhat smaller than most values used previously. This leads to a somewhat lower average density of levels near the Fermi surface, which in turn leads to single-particle corrections of larger amplitude. Since the present potential radius is obtained from statistical calculations that reproduce

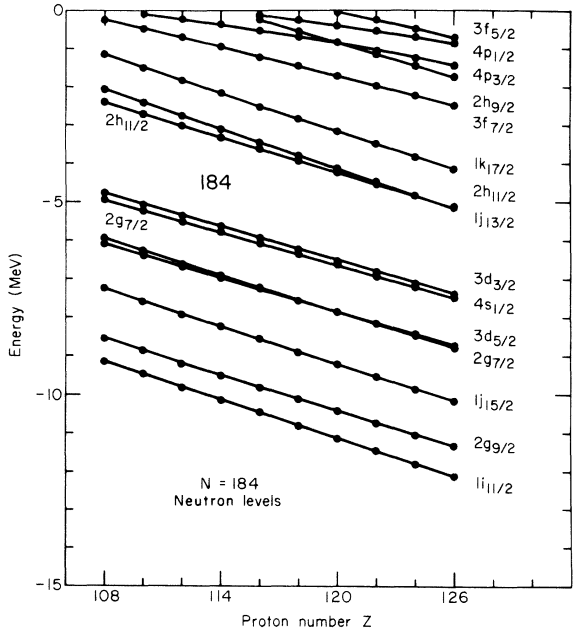

FIG. 16. Dependence of spherical neutron levels upon proton number for superheavy nuclei containing 184 neutrons.

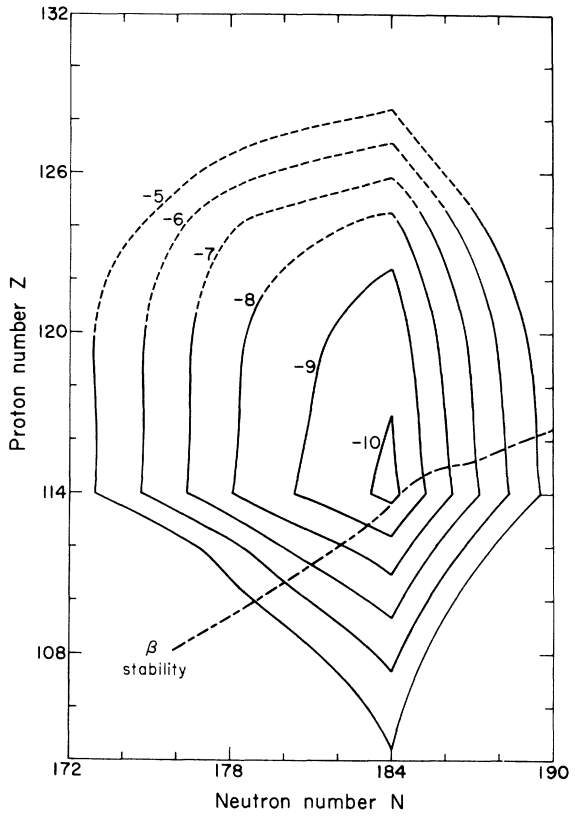

FIG. 17. Contour plot of single-particle correction for spherical superheavy nuclei. The portions of contour lines shown dashed correspond to proton-unstable nuclei. The dot-dashed curve gives the calculated line of β stability.

correctly the average trends throughout the Periodic Table of a variety of nuclear properties,[96] it should be more reliable than a potential radius extrapolated from results adjusted to best reproduce experimental single-particle levels. Results qualitatively similar to ours are also obtained in some other recent calculations.[30,54] (Fission barriers for superheavy nuclei have also been calculated in Refs. 76 and 154–156 by the inadequate method of summing single-particle energies.)

To summarize briefly, the present results suggest that (1) the fission barriers of superheavy nuclei near $^{298}114$ are even higher than previously supposed, (2) the addition of neutrons beyond 184 decreases the barrier height more than subtracting the same number of neutrons from 184, and (3) the addition of several protons beyond 114 has little effect on the fission barriers (although the probability for α decay increases substantially).

VII. SUMMARY AND CONCLUSION

We have performed a new calculation of the nuclear potential energy of deformation, with an emphasis on techniques that permit more accurate extrapolations both to large deformations and to new regions of nuclei. Our calculation proceeds according to the following five steps:

(1) The over-all geometrical shape of the nucleus is specified with five degrees of freedom, in terms of smoothly joined portions of three quadratic surfaces of revolution (e.g., two spheroids connected by a hyperboloidal neck).

(2) The single-particle potential is obtained by folding a Yukawa function with a uniform sharp-surface generating potential of appropriate shape. The parameters describing the potential are obtained from statistical (Thomas-Fermi) calculations that reproduce correctly the average trends throughout the Periodic Table of a variety of nuclear properties.

(3) The Schrödinger equation with this potential is solved for the single-particle energies and wave functions by an expansion of the wave function in a set of deformed harmonic-oscillator basis functions. We also investigated a finite-difference method of solution.

(4) Shell and pairing corrections are calculated from the single-particle energies by use of the methods developed by Strutinsky.

(5) These corrections are added to the surface and Coulomb energies of the liquid-drop model to obtain the total potential energy of deformation.

With this approach we have calculated a limited number of results for heavy and superheavy nuclei. The calculations reproduce the over-all trends of experimental single-particle corrections and quadrupole moments of nuclei in their ground states. They also describe correctly the general region of nuclei whose fission barriers are known experimentally to contain deep secondary minima, as well as the over-all trends of experimental fission-barrier heights of nuclei ranging from rare earths to actinides. The over-all variation in the relative heights of the two peaks in the fission barriers of actinide nuclei agrees with experimental results, but the calculated first peak is somewhat low for thorium isotopes and somewhat high for curium isotopes. The calculated heights of the secondary minimum are in approximate agreement with the experimental heights, but vary more rapidly with neutron number than the experimental heights.

The approach also provides an approximate understanding of experimental fission-fragment mass distributions on the basis of calculated saddle-point shapes. In particular, asymmetric mass distributions for the low-energy fission of actinide nuclei, and the transitions to symmetric distributions for both lighter nuclei like ^{188}Os and heavier nuclei like ^{258}Fm, as well as at high excitation energies, can be understood. The exact location of the transition to symmetric divisions for lighter nuclei and the presence of both symmetric and asymmetric saddle points for nuclei like radium in the transition region are not reproduced. There is some evidence that single-particle effects beyond the saddle point are also important in determining the mass distribution.

There are still some unanswered questions, and more work needs to be done before a final assessment can be made, but tentatively it appears that the combined macroscopic-microscopic method as formulated here does provide a suitable framework for calculating the nuclear potential energy of deformation.

When these same general methods are applied to superheavy nuclei, we find that the fission barriers of nuclei near $^{298}114$ are even higher than previously supposed. With respect to spontaneous fission, the appearance of the island of superheavy nuclei is a mountain ridge extending north and south from 114 protons to about 124 protons. The descent from the mountain down to the sea of instability is rather gentle toward the west (that is, for decreasing neutron numbers below 184). However, east of 184 neutrons, as well as north of 124 protons and south of 114 protons, the descent is more rapid. Nature has been very kind in extending the island both to the north and to the west, since it is the northwest territory that is most accessible experimentally.

The methods discussed here for calculating the nuclear potential energy of deformation have an enormous range of applicability, of which only a

small fraction has been exploited thus far. In future applications, higher-order terms in the macroscopic part of the energy, such as compressibility and curvature effects, should be taken into account, and also an internally consistent set of parameters should be used for both the macroscopic and microscopic parts of the energy. At that point a better assessment of the macroscopic-microscopic approach can be made by using a single method for the systematic calculation of a variety of phenomena. This should include a thorough survey of fission barriers, nuclear ground-state masses and deformations, and the potential energy for heavy-ion reactions. In this way the related areas of fission, nuclear masses, and heavy-ion physics can be unified, and a sense of continuity achieved in the development of their theory.

ACKNOWLEDGMENTS

We would like to acknowledge stimulating discussions concerning this work with many of our colleagues. In particular, H. C. Britt, W. D. Myers, W. J. Swiatecki, and S. Wahlborn have had major impacts on the directions the work has taken.

APPENDIX: NUMERICAL ACCURACY OF THE CALCULATIONS

A. Single-Particle Energies and Wave Functions

Since the numerical accuracy of the finite-difference method of solution is discussed in Ref. 93, we limit ourselves here to the accuracy of the expansion in deformed harmonic-oscillator basis functions. The primary source of error in calculating the single-particle energies and wave functions is the truncation of the basis. Integration errors involved in calculating the matrix elements, and matrix-diagonalization errors can in practice be made negligibly small compared to the truncation error.

Figure 18 illustrates the dependence of the single-particle energies on the size of the basis. The calculated energies for various spherical neutron levels in ^{208}Pb are plotted vs $1/N_0$, where N_0 is the number of harmonic-oscillator quanta included in the basis. In this plot the results become more accurate toward the left, with the limit of an infinite basis given by $1/N_0 = 0$. Levels below the Fermi surface converge fairly rapidly with the size of the basis, whereas bound levels close to zero energy converge less rapidly. *The unbound levels approach 0 as the basis becomes infinite.* This is because any positive energy is a solution of the Schrödinger equation; to simulate the continuum, the density of unbound levels approaches infinity as the basis becomes infinite. Thus, the unbound levels calculated with a finite basis do *not* represent resonant states, as is often suggested. Nevertheless, they are of use in calculating the shell correction, as we discuss in Appendix B.

In addition to a spherical ^{208}Pb nucleus, we have tested the convergence of the single-neutron and single-proton energies for ^{240}Pu for the symmetric deformation $y = 0.24$, for the case of two equal tangent spheres, and for a very asymmetric case corresponding to the $x = 0.8$ Businaro-Gallone saddle point.[75,158] For a sphere, the results were checked with those calculated by use of the shooting method,[99,103-107] and for general shapes with those calculated by use of the finite-difference method.[81,92,93] Except for the very asymmetric shape, we found that the truncation error corresponding to $N_0 = 12$ is in general about 0.001 MeV for the ground state, 0.1 MeV for the Fermi surface, and 0.3 MeV for the least-bound level. (The truncation errors for the Fermi surface and least-bound level are larger in cases where these levels are closer to 0.) For the very asymmetric shape, the truncation errors are substantially larger.

For potentials that go to zero at large distances, the true asymptotic behavior of the bound-state wave functions is exponential, whereas the asymptotic behavior of wave functions calculated in an oscillator expansion is Gaussian. This is illustrated in Fig. 19 for the neutron Fermi surface and least-bound level in a spherical ^{208}Pb nucleus. In such a semilogarithmic plot of r times the radial wave function vs r, errors in the asymptotic behavior appear as deviations from a straight line. The wave function for the Fermi surface is calculated accurately out to 12 fm for a basis containing states up to 12 quanta, and fairly accurately out to 15 fm for 24 quanta. This is 4.5 and 7.5 fm, respectively, beyond the radius at which the value of the potential is $\frac{1}{2}$ its maximum value. At these distances, the wave function (times r) has decreased to about 10 and 2%, respectively, of its maximum value. The wave function for the least-bound level is calculated accurately out to only 9 fm, where the wave function is still about 90% of its maximum value, for both 12 quanta and 24 quanta.

B. Shell and Pairing Corrections

Apart from fundamental questions associated with the over-all validity of the method itself, the numerical accuracy with which the shell correction can be calculated is limited solely by the accuracy with which the smooth curve $\bar{\epsilon}(n)$ of Fig. 6 can be determined *below* the Fermi surface $\bar{\lambda}$. For a given set of single-particle energies, the smooth curve is determined so as to remove the local fluctuations of the energies but retain their long-range

behavior. Strutinsky's method provides a means for determining the smooth curve, but it depends upon both the smoothing range γ and the order p. This in turn leads to a dependence of the shell correction upon these quantities.

This dependence is illustrated in Fig. 20 for neutrons in a spherical ^{208}Pb nucleus, when a basis containing states up to 12 oscillator quanta is used. For small values of γ, the shell correction is close to zero, since the smooth curve of Fig. 6 is close to the staircase curve. For values of γ close to $\hbar\omega_0$, the shell correction is relatively insensitive to both the value of γ and the order p. This is because neither γ nor p represent physical quantities. As long as the smoothing range is close to the spacing between major shells and the order is not too large, the shell correction depends only weakly upon their precise values. For moderately large values of γ (several $\hbar\omega_0$), an increase in γ causes the shell correction to become more negative. As γ continues to increase, the shell correction goes through a minimum and finally diverges to $+\infty$ as γ approaches ∞, in accordance with the results of Lin.[127]

The results shown in Fig. 20 are qualitatively similar to those obtained previously for a harmonic-oscillator potential,[40,41] but differ from the results of Lin[127] and Brueckner[128] for a diffuse-surface potential that goes to zero at large distances. In the latter work, the density of levels in the continuum is spuriously low, which causes the shell correction to diverge to $+\infty$ by going through a minimum only (rather than through a plateau) as γ increases. This behavior in turn led Lin and Brueckner to conclude erroneously that the Strutinsky shell-correction method could not be applied to potentials that go to zero at large distances.

The effect of the density of unbound states on the shell correction is illustrated in Fig. 21. This is a plot of the neutron shell correction for a spherical ^{208}Pb nucleus as a function of $1/N_0$, for $\gamma = 1.0\hbar\omega_0$. For moderate values of $1/N_0$ (corresponding to $8 \lesssim N_0 \lesssim 13$), the shell correction is relatively insensitive to the size of basis used. However, as $1/N_0$ approaches 0, the shell correction diverges to $+\infty$. This is because, as we saw in Fig. 18, the density of unbound states approaches ∞ as $1/N_0$ approaches 0. This lowers the smooth curve of Fig. 6, which in turn increases the shell correction. Since the effect of the unbound states is larger for larger values of γ, the shell correc-

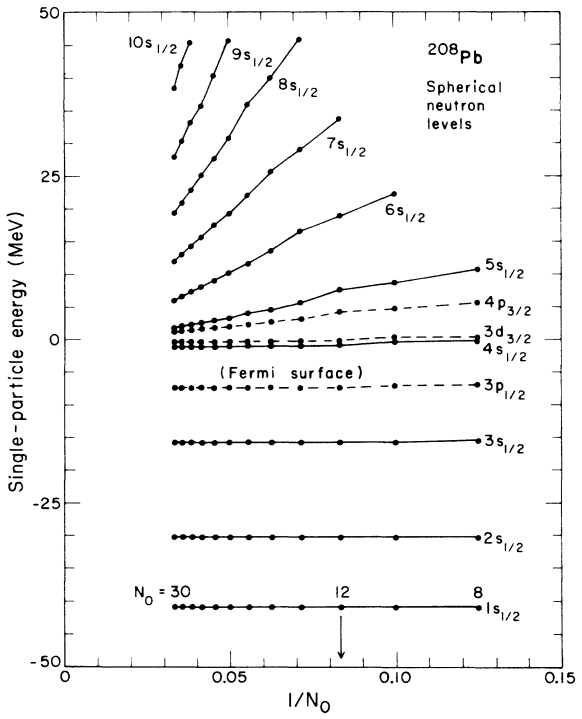

FIG. 18. Dependence of spherical neutron levels of ^{208}Pb upon $1/N_0$, where N_0 is the number of harmonic-oscillator quanta included in the basis. In addition to s states, which are shown as solid lines, the Fermi surface, the least-bound level, and the least-unbound level (for $N_0 = 30$) are also included as dashed lines. The arrow indicates the number of quanta (12) used in most of our calculations.

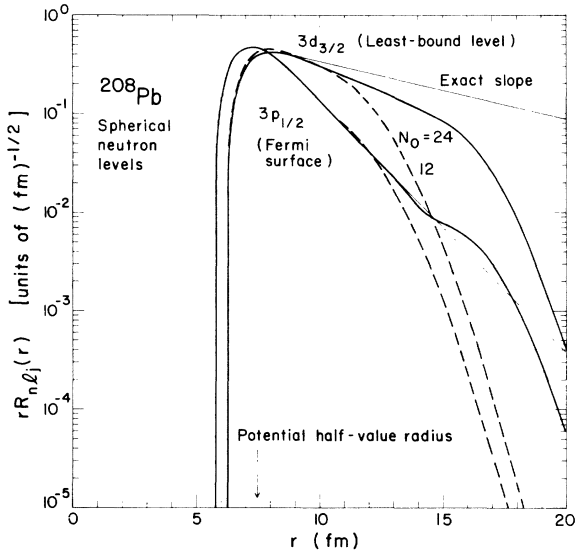

FIG. 19. Asymptotic behavior of neutron wave functions for a spherical ^{208}Pb nucleus. The product of r times the radial wave function is plotted vs r beyond the last node for the Fermi surface and the least-bound level. The thin solid straight lines give the exact slopes, the heavy solid curves the results for a harmonic-oscillator basis containing states up to 24 quanta, and the dashed curves the results for a basis containing states up to 12 quanta. The arrow indicates the radius at which the value of the single-particle potential is $\frac{1}{2}$ its depth.

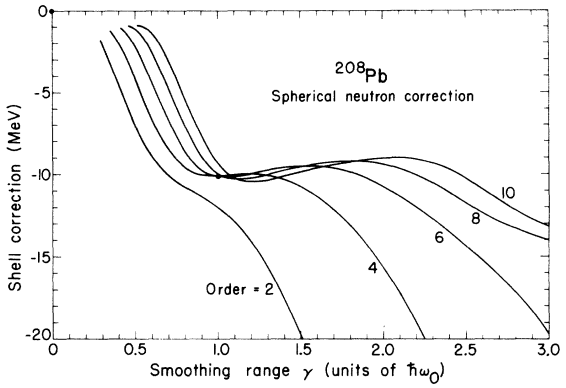

FIG. 20. Dependence of spherical neutron shell correction for ^{208}Pb upon smoothing range γ, for various orders. The solid point on the sixth-order curve at $\gamma = 1.0\hbar\omega_0 = 41\ \mathrm{MeV}/A^{1/3}$ indicates the values used in our calculations. For small smoothing ranges, multiple solutions exist; these are not included in the figure, but the solid point at the origin gives the single solution for $\gamma = 0$. All single-particle levels from a harmonic-oscillator basis containing states up to 12 quanta are used.

tion diverges to $+\infty$ more rapidly than the curve of Fig. 21 when $\gamma > 1.0\hbar\omega_0$, and less rapidly when $\gamma < 1.0\hbar\omega_0$.

From Figs. 20 and 21 and similar results for other cases, we conclude that for a given single-particle potential, the Strutinsky shell correction can be computed with a numerical accuracy of

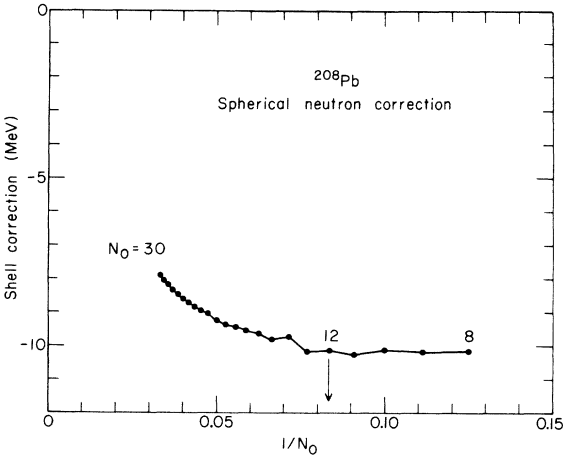

FIG. 21. Dependence of spherical neutron shell correction for ^{208}Pb upon $1/N_0$, where N_0 is the number of harmonic-oscillator quanta included in the basis. The results are calculated with a sixth-order correction and smoothing range $\gamma = 1.0\hbar\omega_0 = 41\ \mathrm{MeV}/A^{1/3}$. The arrow indicates the number of quanta (12) used in our calculations of single-particle corrections.

about 0.5 MeV, except for light nuclei. The low density of levels in light nuclei makes it more difficult to determine the smooth curve $\bar{\epsilon}(n)$ of Fig. 6, which in turn reduces the accuracy with which the shell correction can be calculated.[122, 159]

Apart from fundamental questions associated with the treatment of the pairing interaction in terms of a constant interaction strength and the use of the BCS approximation, the numerical accuracy with which the pairing correction can be calculated is limited primarily by the sensitivity of the results to the number of pairs included in the calculation. As shown in Fig. 22, the pairing correction ΔE_{pc} and other quantities of interest depend sensitively upon the number of pairs N_p only for small values of N_p. When a moderate or large number of pairs are included, the results are very insensitive to the precise number used. [The replacement of the smooth curve $\bar{\epsilon}(n)$ in Fig. 6 by a straight line over the region considered in the pairing calculation leads to a small systematic error.] From these and similar results, we conclude that for a given single-particle potential and value of $\bar{\Delta}$, the pairing correction can be calculated with a numerical accuracy of about 0.1 MeV, except for light nuclei. The smaller number of pairs present in light nuclei reduces the accuracy with which the pairing correction can be calculated.

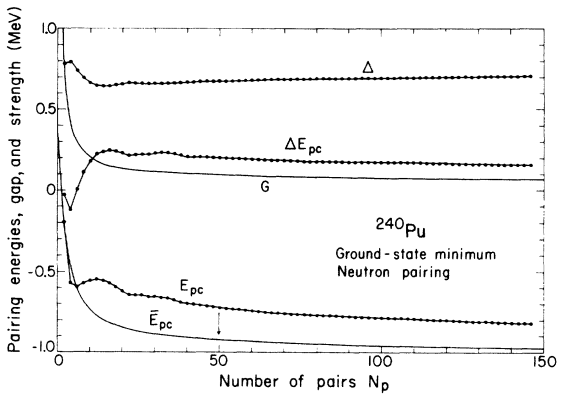

FIG. 22. Various neutron pairing quantities for ^{240}Pu at its spheroidal ground-state minimum, as functions of the number of pairs included in the calculation. The upper smooth curve gives the pairing strength G required to reproduce an average pairing gap $\bar{\Delta} = 12\ \mathrm{MeV}/A^{1/2}$, and the lower smooth curve gives the average pairing correlation energy $\bar{E}_{pc}$. The upper solid points (connected by straight lines) give the pairing gap Δ, the lower solid points the pairing correlation energy E_{pc}, and the middle solid points the pairing correction $\Delta E_{pc} = E_{pc} - \bar{E}_{pc}$. The arrow indicates the number of pairs (50) having negative energy with equal numbers above and below the Fermi surface.

*Work performed under the auspices of the U. S. Atomic Energy Commission.

†Present address: Kellogg Radiation Laboratory, California Institute of Technology, Pasadena, California 91109.

[1]W. J. Swiatecki, in *Proceedings of the Second International Conference on Nuclidic Masses, Vienna, 1963* (Springer, Vienna, 1964), p. 58.

[2]V. M. Strutinsky, Yadern. Fiz. 3, 614 (1966) [transl.: Soviet J. Nucl. Phys. 3, 449 (1966)].

[3]W. D. Myers and W. J. Swiatecki, Nucl. Phys. 81, 1 (1966).

[4]W. D. Myers and W. J. Swiatecki, Arkiv Fysik 36, 343 (1967).

[5]C. Y. Wong, Phys. Letters 21, 688 (1966).

[6]A. M. Friedman, Joint Institute for Nuclear Research Report No. JINR-D7-3548, 1967 (unpublished), p. 39.

[7]V. M. Strutinsky and Yu. A. Muzychka, Joint Institute for Nuclear Research Report No. JINR-D7-3548, 1967 (unpublished), p. 51.

[8]V. M. Strutinsky, Institute of Atomic Energy Report No. IAE-1108, 1966 (unpublished) [transl.: ANL Report No. ANL-TRANS-353, 1966 (unpublished)].

[9]V. M. Strutinsky, Arkiv Fysik 36, 629 (1967).

[10]V. M. Strutinsky, Institute of Atomic Energy Report No. IAE-1350, 1967 (unpublished) [transl.: LASL Report No. LA-TR-67-36, 1967 (unpublished)].

[11]V. M. Strutinsky, Nucl. Phys. A95, 420 (1967).

[12]V. M. Strutinsky, Nucl. Phys. A122, 1 (1968).

[13]Yu. A. Muzychka, V. V. Pashkevich, and V. M. Strutinsky, Yadern. Fiz. 8, 716 (1968) [transl.: Soviet J. Nucl. Phys. 8, 417 (1969)].

[14]V. V. Pashkevich, Joint Institute for Nuclear Research Report No. JINR-P4-4383, 1969 (unpublished).

[15]V. V. Pashkevich, Joint Institute for Nuclear Research Report No. JINR-D-3893, 1968 (unpublished), p. 94.

[16]V. M. Strutinsky and S. Bjørnholm, in *Proceedings of the International Symposium on Nuclear Structure, Dubna, 1968* (International Atomic Energy Agency, Vienna, 1968), p. 431.

[17]V. V. Pashkevich and V. M. Strutinsky, Yadern. Fiz. 9, 56 (1969) [transl.: Soviet J. Nucl. Phys. 9, 35 (1969)].

[18]Yu. A. Muzychka, Phys. Letters 28B, 539 (1969).

[19]Yu. A. Muzychka, Yadern. Fiz. 10, 113 (1969) [transl.: Soviet J. Nucl. Phys. 10, 66 (1970)].

[20]Yu. A. Muzychka, Yadern. Fiz. 11, 105 (1970) [transl.: Soviet J. Nucl. Phys. 11, 57 (1970)].

[21]V. V. Pashkevich, Nucl. Phys. A133, 400 (1969).

[22]J. Damgaard, H. C. Pauli, V. V. Pashkevich, and V. M. Strutinsky, Nucl. Phys. A135, 432 (1969).

[23]S. Bjørnholm and V. M. Strutinsky, Nucl. Phys. A136, 1 (1969).

[24]V. M. Strutinsky and H. C. Pauli, in *Proceedings of the Second International Atomic Energy Agency Symposium on Physics and Chemistry of Fission, Vienna, Austria, 1969* (International Atomic Energy Agency, Vienna, 1969), p. 155.

[25]V. M. Strutinsky, in *Proceedings of the Robert A. Welch Foundation Conference XIII. The Transuranium Elements, Houston, Texas, 1969* (Robert A. Welch Foundation, Houston, Texas, 1970), p. 83.

[26]S. Bjørnholm, in *Proceedings of the Robert A. Welch Foundation Conference XIII. The Transuranium Elements, Houston, Texas,* 1969 (see Ref. 25), p. 447.

[27]H. C. Pauli, T. Ledergerber, and M. Brack, Phys. Letters 34B, 264 (1971).

[28]H. C. Pauli and T. Ledergerber, to be published.

[29]V. V. Pashkevitch, Joint Institute for Nuclear Research Report No. JINR-P4-5581, 1971 (unpublished) [transl.: ANL Report No. ANL-TRANS-878, 1971 (unpublished)].

[30]M. Brack, J. Damgaard, H. C. Pauli, A. Stenholm-Jensen, V. M. Strutinsky, and C. Y. Wong, to be published.

[31]P. A. Seeger and R. C. Perisho, LASL Report No. LA-3751, 1967 (unpublished).

[32]P. A. Seeger, in *Proceedings of the Third International Conference on Atomic Masses, Winnipeg, 1967* (University of Manitoba Press, Winnipeg, 1967), p. 85.

[33]P. A. Seeger, CERN Report No. CERN 70-30, 1970 (unpublished), Vol. 1, p. 217.

[34]P. A. Seeger, LASL Report No. LA-DC-12792, 1971 (to be published).

[35]S. G. Nilsson and J. R. Nix, Bull. Am. Phys. Soc. 13, 605 (1968).

[36]S. G. Nilsson and J. R. Nix, Joint Institute for Nuclear Research Report No. JINR-D-3893, 1968 (unpublished), p. 86.

[37]S. G. Nilsson, J. R. Nix, A. Sobiczewski, Z. Szymański, S. Wycech, C. Gustafsson, and P. Möller, Nucl. Phys. A115, 545 (1968).

[38]S. G. Nilsson, in *Cargèse Lectures in Physics,* edited by M. Jean (Gordon and Breach, New York, 1969), Vol. 3, p. 105.

[39]S. G. Nilsson, S. G. Thompson, and C. F. Tsang, Phys. Letters 28B, 458 (1969).

[40]S. G. Nilsson, C. F. Tsang, A. Sobiczewski, Z. Szymański, S. Wycech, C. Gustafsson, I. L. Lamm, P. Möller, and B. Nilsson, Nucl. Phys. A131, 1 (1969).

[41]C. F. Tsang, Ph.D. thesis, University of California, 1969 (unpublished); UCRL Report No. UCRL-18899, 1969 (unpublished).

[42]S. G. Nilsson, in *Proceedings of the International Conference on Properties of Nuclear States, Montreal, 1969* (University of Montreal Press, Montreal, 1969), p. 149.

[43]P. Möller, S. G. Nilsson, A. Sobiczewski, Z. Szymański, and S. Wycech, Phys. Letters 30B, 223 (1969).

[44]S. G. Nilsson, G. Ohlén, C. Gustafsson, and P. Möller, Phys. Letters 30B, 437 (1969).

[45]C. F. Tsang and S. G. Nilsson, Nucl. Phys. A140, 275 (1970).

[46]C. F. Tsang and S. G. Nilsson, Nucl. Phys. A140, 289 (1970).

[47]P. Möller, Nucl. Phys. A142, 1 (1970).

[48]P. Möller and S. G. Nilsson, Phys. Letters 31B, 171 (1970).

[49]P. Möller and S. G. Nilsson, Phys. Letters 31B, 283 (1970).

[50]C. F. Tsang and S. G. Nilsson, CERN Report No. CERN 70-30, 1970 (unpublished), Vol. 2, p. 769.

[51]R. Bengtsson, C. Gustafsson, T. Johansson, P. Möller, S. G. Nilsson, G. Ohlén, and I. Ragnarsson, CERN Report No. CERN 70-30, 1970 (unpublished), Vol. 2, pp. 645, 847.

[52]C. Gustafsson, P. Möller, and S. G. Nilsson, Phys. Letters 34B, 349 (1971).

[53]T. Johansson, S. G. Nilsson, and Z. Szymański, Ann. Phys. (Paris) 5, 377 (1970).

[54]A. Lukasiak, A. Sobiczewski, and W. Stępień-Rudzka, Institute of Nuclear Research Report No. INR-P-1293/VII/PL, 1971 (to be published); A. Sobiczewski, private communication.
[55]K. Albrecht, D. Scharnweber, W. Greiner, and U. Mosel, Phys. Letters 32B, 229 (1970).
[56]U. Mosel and D. Scharnweber, Phys. Rev. Letters 25, 678 (1970).
[57]K. Albrecht, D. Scharnweber, and W. Greiner, CERN Report No. CERN 70-30, 1970 (unpublished), Vol. 2, p. 775.
[58]J. Grumann, T. Morović, and W. Greiner, Z. Naturforsch. 26a, 643 (1971).
[59]D. Scharnweber, W. Greiner, and U. Mosel, Nucl. Phys. A164, 257 (1971).
[60]U. Mosel and H. W. Schmitt, Nucl. Phys. A165, 73 (1971).
[61]U. Mosel and H. W. Schmitt, Bull. Am. Phys. Soc. 16, 516 (1971).
[62]U. Mosel and H. W. Schmitt, Phys. Rev. C 4, 2185 (1971).
[63]B. L. Anderson, F. Dickmann, and K. Dietrich, Nucl. Phys. A159, 337 (1970).
[64]K. Dietrich, to be published.
[65]G. D. Adeev, P. A. Cherdantsev, and I. A. Gamalya, Phys. Letters 35B, 125 (1971).
[66]H. J. Krappe and U. Wille, in *Proceedings of the Second International Atomic Energy Agency Symposium on Physics and Chemistry of Fission, Vienna, 1969* (see Ref. 24), p. 197.
[67]J. R. Nix, CERN Report No. CERN 70-30, 1970 (unpublished), Vol. 2, p. 605.
[68]J. R. Nix, LASL Report No. LA-DC-12488, 1971 (unpublished).
[69]M. Bolsterli, E. O. Fiset, J. R. Nix, and J. L. Norton, Phys. Rev. Letters 27, 681 (1971).
[70]J. L. Norton, J. R. Nix, and M. Bolsterli, in *American Chemical Society Abstracts of Papers, 162nd Meeting* (American Chemical Society, Washington, D. C., 1971), abstract NUCL 1.
[71]C. Y. Wong, to be published.
[72]H. Schultheis, R. Schultheis, and G. Süssmann, Nucl. Phys. A144, 545 (1970).
[73]H. Schultheis and R. Schultheis, Phys. Letters 34B, 245 (1971).
[74]H. Schultheis and R. Schultheis, Phys. Letters 35B, 296 (1971).
[75]J. R. Nix, Nucl. Phys. A130, 241 (1969); UCRL Report No. UCRL-17958, 1968 (unpublished).
[76]C. Gustafsson, I. L. Lamm, B. Nilsson, and S. G. Nilsson, Arkiv Fysik 36, 613 (1967).
[77]S. G. Nilsson, in *Proceedings of the International School of Physics "Enrico Fermi," Nuclear Structure and Nuclear Reactions, Course XL, Varenna, 1967,* edited by M. Jean and R. A. Ricci (Academic, New York, 1969), p. 142.
[78]A. Brandt and I. Kelson, Phys. Rev. 183, 1025 (1969).
[79]M. Gaudin and A. M. Sajot, in *Proceedings of the International Atomic Energy Agency Symposium on Physics and Chemistry of Fission, Vienna, 1969* (see Ref. 24), p. 229.
[80]P. Röper, Z. Physik 195, 316 (1966).
[81]F. Dickmann, Z. Physik 203, 141 (1967).
[82]J. Bennewitz and P. K. Haug, Z. Physik 212, 295 (1968).
[83]P. Holzer, U. Mosel, and W. Greiner, Nucl. Phys. A138, 241 (1969).
[84]W. Greiner, in *Proceedings of the International Conference on Nuclear Reactions Induced by Heavy Ions, Heidelberg, Germany, 1969* (North-Holland, Amsterdam, 1970), p. 748.
[85]D. Scharnweber, U. Mosel, and W. Greiner, Phys. Rev. Letters 24, 601 (1970).
[86]U. Mosel, J. Maruhn, and W. Greiner, Phys. Letters 34B, 587 (1971).
[87]J. Maruhn and W. Greiner, to be published.
[88]C. Y. Wong, Phys. Letters 30B, 61 (1969).
[89]U. Götz, H. C. Pauli, and K. Alder, to be published.
[90]W. Ogle, S. Wahlborn, R. Piepenbring, and S. Fredriksson, Rev. Mod. Phys. 43, 424 (1971).
[91]G. Ehrling and S. Wahlborn, Phys. Letters 34B, 369 (1971).
[92]M. Bolsterli, E. O. Fiset, and J. R. Nix, in *Proceedings of the Second International Atomic Energy Agency Symposium on Physics and Chemistry of Fission, Vienna, 1969* (see Ref. 24), p. 183.
[93]E. O. Fiset, J. R. Nix, and M. Bolsterli, LASL Report No. LA-4735-MS, 1971 (unpublished).
[94]J. D. Talman, Phys. Rev. 102, 455 (1956).
[95]C. Syros, Ph.D. dissertation, University of Cologne, 1961 (unpublished).
[96]W. D. Myers, Nucl. Phys. A145, 387 (1970).
[97]D. L. Hill and J. A. Wheeler, Phys. Rev. 89, 1102 (1953).
[98]W. J. Swiatecki, in *Proceedings of the Second United Nations International Conference on the Peaceful Uses of Atomic Energy, Geneva, 1958* (United Nations, Geneva, 1958), Vol. 15, p. 248.
[99]J. Blomqvist and S. Wahlborn, Arkiv Fysik 16, 545 (1960).
[100]M. Bolsterli and J. L. Norton, J. Math. Phys. 12, 969 (1971).
[101]J. Ortega, in *Mathematical Methods for Digital Computers,* edited by A. Ralston and H. S. Wilf (Wiley, New York, 1967), Vol. II, Chap. 4, pp. 94–115.
[102]S. G. Nilsson, Kgl. Danske Videnskab. Selskab, Mat.-Fys. Medd. 29, No. 16 (1955).
[103]G. E. Brown, J. H. Gunn, and P. Gould, Nucl. Phys. 46, 598 (1963).
[104]J. M. Blatt, J. Computational Phys. 1, 382 (1967).
[105]I. H. Sloan, J. Computational Phys. 2, 414 (1968).
[106]E. Rost, Phys. Rev. 154, 994 (1967).
[107]R. L. Tarp, UCRL Report No. UCRL-50430, 1968 (unpublished).
[108]W. D. Myers and W. J. Swiatecki, Ann. Phys. (N.Y.) 55, 395 (1969).
[109]W. D. Myers and W. J. Swiatecki, UCRL Report No. UCRL-19543, 1970 (unpublished).
[110]W. D. Myers, University of California, Lawrence Berkely Laboratory Report No. LBL-209, 1971 (to be published).
[111]R. W. Hasse, UCRL Report No. UCRL-19910, 1970 (to be published).
[112]J. W. Truran, A. G. W. Cameron, and E. Hilf, CERN Report No. CERN 70-30, 1970 (unpublished), Vol. 1, p. 275.

[113]S. Ludwig, H. von Groote, E. Hilf, A. G. W. Cameron, and J. Truran, to be published.
[114]A. S. Tyapin, Yadern. Fiz. 11, 98 (1970)[transl.: Soviet J. Nucl. Phys. 11, 53 (1970)].
[115]W. H. Bassichis, A. K. Kerman, C. F. Tsang, D. R. Tuerpe, and L. Wilets, University of California, Lawrence Livermore Laboratory Report No. UCRL-73044, 1971 (to be published).
[116]H. A. Bethe, to be published.
[117]M. L. Gursky, Ph.D. thesis, Vanderbilt University, 1958 (unpublished); private communication.
[118]M. Bolsterli, unpublished results.
[119]W. D. Myers and W. J. Swiatecki, unpublished results.
[120]E. Hilf, to be published.
[121]R. Balian and C. Bloch, Centre d'Études Nucléaires de Saclay Report No. DPh-T/71-16, 1971 (to be published).
[122]V. A. Ramamurthy, S. S. Kapoor, and S. K. Kataria, Phys. Rev. Letters 25, 386 (1970); S. S. Kapoor, private communication.
[123]R. K. Bhaduri and C. K. Ross, Phys. Rev. Letters 27, 606 (1971).
[124]H. A. Bethe, Rev. Mod. Phys. 9, 69 (1937).
[125]T. Ericson, Advan. Phys. 9, 425 (1960).
[126]A. Bohr and B. Mottelson, *Nuclear Structure* (Benjamin, New York, 1969), Vol. I, pp. 281–293.
[127]W. Lin, Phys. Rev. C 2, 871 (1970).
[128]K. A. Brueckner, CERN Report No. CERN 70-30, 1970 (unpublished), Vol. 2, p. 773.
[129]S. T. Belyaev, Kgl. Danske Videnskab. Selskab, Mat.-Fys. Medd. 31, No. 11 (1959).
[130]A. Bohr and B. Mottelson, *Nuclear Structure* (Benjamin, New York, 1969), Vol. I, p. 170.
[131]N. Zeldes, A. Grill, and A. Simievic, Kgl. Danske Videnskab. Selskab, Mat.-Fys. Skrifter 3, No. 5 (1967).
[132]H. C. Britt, W. R. Gibbs, J. J. Griffin, and R. H. Stokes, Phys. Rev. 139, B354 (1965).
[133]J. R. Huizenga, A. N. Behkami, J. W. Meadows, Jr., and E. D. Klema, Phys. Rev. 174, 1539 (1968).
[134]G. N. Smirenkin, V. G. Nesterov, and A. S. Tishin, Yadern. Fiz. 6, 921 (1967) [transl.: Soviet J. Nucl. Phys. 6, 671 (1968)].
[135]A. V. Ignatyuk and G. N. Smirenkin, Phys. Letters 29B, 159 (1969).
[136]K. D. Androsenko, S. B. Ermagambetov, A. V. Ignatyuk, N. S. Rabotnov, G. N. Smirenkin, A. S. Soldatov, L. N. Usachev, D. L. Shpak, S. P. Kapitsa, Iu. M. Tsipeniuk, and I. Kovach, Obninsk Report No. FEI-185, 1969 (unpublished) [transl.: LASL Report No. LA-4369-TR, 1970 (unpublished)].
[137]R. C. Kennedy, Phys. Rev. 144, 804 (1966).
[138]J. von Neumann and E. Wigner, Physik. Z. 30, 467 (1929).
[139]E. Teller, J. Phys. Chem. 41, 109 (1937).
[140]C. A. Coulson and J. T. Lewis, in *Quantum Theory*, edited by D. R. Bates (Academic, New York, 1962), Vol. II, pp. 203–205.
[141]H. Eyring, J. Walter, and G. E. Kimball, *Quantum Chemistry* (Wiley, New York, 1949), pp. 205–206.
[142]K. E. G. Löbner, M. Vetter, and V. Hönig, Nucl. Data A7, 495 (1970).
[143]W. J. Swiatecki, unpublished results.
[144]J. E. Lynn, in *Proceedings of the Second International Atomic Energy Agency Symposium on Physics and Chemistry of Fission, Vienna, 1969* (see Ref. 24), p. 249.
[145]H. C. Britt, S. C. Burnett, B. H. Erkkila, J. E. Lynn, and W. E. Stein, Phys. Rev. C 4, 1444 (1971).
[146]A. Khodai-Joopari, Ph.D. thesis, University of California, 1966 (unpublished); UCRL Report No. UCRL-16489, 1966 (unpublished).
[147]S. G. Thompson *et al.*, unpublished results.
[148]Discussion in *Proceedings of the Robert A. Welch Foundation Conference XIII. The Transuranium Elements, Houston, Texas, 1969* (see Ref. 25), pp. 206–211.
[149]W. J. Swiatecki, unpublished results.
[150]L. Wilets, *Theories of Nuclear Fission* (Clarendon, Oxford, 1964), p. 8.
[151]J. P. Balagna, G. P. Ford, D. C. Hoffman, and J. D. Knight, Phys. Rev. Letters 26, 145 (1971).
[152]W. John, E. K. Hulet, R. W. Lougheed, and J. J. Wesolowski, Phys. Rev. Letters 27, 45 (1971).
[153]R. W. Hasse, Nucl. Phys. A128, 609 (1969).
[154]U. Mosel and W. Greiner, Z. Physik 222, 261 (1969).
[155]J. Grumann, U. Mosel, B. Fink, and W. Greiner, Z. Physik 228, 371 (1969).
[156]R. Fraser, J. Grumann, and W. Greiner, Phys. Letters 35B, 483 (1971).
[157]W. H. Bassichis and L. Wilets, Phys. Rev. Letters 22, 799 (1969).
[158]U. L. Businaro and S. Gallone, Nuovo Cimento 5, 315 (1957).
[159]J. R. Huizenga and F. C. Williams, Jr., unpublished results.

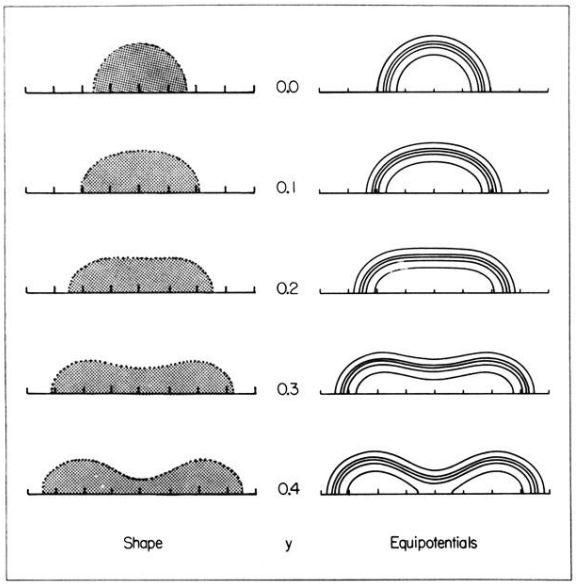

FIG. 4. Shapes described by the symmetric-deformation coordinate y, and resulting equipotentials of the folded Yukawa spin-independent nuclear potential V_1. The equipotential curves shown are for 10, 30, 50, 70, and 90% of the well depth V_0.